Uniform asymptotic description of ultrashort rectangular optical pulse propagation in a linear, causally dispersive medium

Kurt Edmund Oughstun*
Department of Computer Science and Electrical Engineering, University of Vermont, Burlington, Vermont 05405

George C. Sherman
Rocketdyne Division, MS FA40, Rockwell International Corporation, 6633 Canoga Avenue, Canoga Park, California 91303
(Received 10 October 1989)

The uniform asymptotic description of the propagation of an input rectangle-modulated harmonic signal of fixed angular frequency ω_c and initial pulse width T into the half-space $z>0$ that is occupied by a single-resonance Lorentz medium is presented. The asymptotic description is developed by representing the input rectangular pulse as the difference between two Heaviside-unit-step-function-modulated signals that are separated in time by the initial pulse width T. This representation clearly shows that the resultant pulse distortion in the dispersive medium is primarily due to the Sommerfeld and Brillouin precursor fields that are associated with the leading and trailing edges of the input pulse. The dynamical pulse evolution with increasing propagation distance $z>0$ is completely described for both long and very short initial pulse widths T. In both cases it is shown that the pulse distortion becomes severe when the propagation distance z is such that the precursor fields associated with the trailing edge of the pulse interfere with the precursor fields associated with the leading edge. Finally, the asymptotic theory clearly shows that the main body of the pulse propagates with the signal velocity in the dispersive medium.

I. INTRODUCTION

The classical theory of optical pulse propagation in a locally linear, homogeneous, isotropic, causally dispersive medium, as described by the Lorentz model, beginning with the seminal analysis of Sommerfeld[1] and Brillouin[2,3] and continuing up to the modern asymptotic analysis of Oughstun and Sherman,[4-6] has provided a complete, rigorous description of the dynamical field evolution for the two canonical problems of the input-unit-step-function-modulated signal of fixed carrier frequency ω_c and the input δ-function pulse. This analysis has focused on the complete precursor field evolution and the precise definition of the signal arrival and has led to a new physical description of dispersive pulse propagation[7] in terms of the energy velocity and attenuation of time-harmonic waves that supplants the previous group-velocity description[8-10] in the mature dispersion regime and reduces to it in the absence of absorption. The accuracy of this uniform asymptotic description in the mature dispersion regime has been completely verified through precise numerical simulations of both the Sommerfeld and Brillouin precursor field evolution[11] and the signal arrival[12] in a single-resonance Lorentz medium. The mature dispersion regime has been found[12] to include all propagation distances z that are greater than one absorption depth in the medium at the signal frequency. When this condition prevails, each quasimonochromatic component of the field propagates with its own characteristic velocity, which remains constant as the propagation continues. At each space-time point $\theta=ct/z$ the propagated field is then dominated by a single real frequency ω_E that is the frequency of the time-harmonic field with the least attenuation that has an energy velocity[13,14] equal to z/t, as described in Ref. 7.

The analysis of the present paper applies this modern asymptotic description to obtain a rigorous, uniformly valid description of rectangular pulse propagation in a single-resonance Lorentz medium in the mature dispersion regime. This approach does not rely upon any quasimonochromatic or slowly varying envelope approximation, as may be found in other descriptions,[15-19] and so yields a canonical description of pulse dispersion phenomena that is completely valid for rapid rise-time pulses of arbitrary time duration. In addition, this approach does not depend upon any nth-order dispersion approximation that is central to other approaches,[20-22] so that it rigorously maintains the complete causality relations[23] that are critical to the proper analysis of linear dispersive pulse dynamics. It is only fair to point out that these other approaches are, in a broad sense, more general in that they are typically applicable to inhomogeneous media. However, what they gain in more general applicability they lose in complete rigor when considering the effects of dispersion on ultrashort pulse dynamics. For convenience, the notation employed in Refs. 5 and 6 is used throughout this paper.

The integral representation of the propagated plane-wave pulse in the half-space $z>0$ is given by[5]

$$A(z,t)=\frac{1}{2\pi}\int_C \tilde{f}(\omega)e^{(z/c)\phi(\omega,\theta)}d\omega\ , \tag{1.1}$$

where

$$\tilde{f}(\omega)=\int_{-\infty}^{\infty} f(t)e^{i\omega t}dt \tag{1.2}$$

is the temporal Fourier spectrum of the initial pulse $f(t)=A(0,t)$ on the plane $z=0$. Here $A(z,t)$ represents either the scalar potential or any scalar component of the electric field, magnetic field, Hertz vector, or vector potential field whose spectral amplitude $A(z,\omega)$ satisfies the dispersive Helmholtz equation

$$[\nabla^2+\tilde{k}^2(\omega)]A(z,\omega)=0 \ . \tag{1.3}$$

The complex wave number $\tilde{k}(\omega)$ is given by

$$\tilde{k}(\omega)=\frac{\omega}{c}n(\omega) \ , \tag{1.4}$$

where the constant c denotes the speed of light in vacuum, and where $n(\omega)=[\epsilon(\omega)]^{1/2}$ is the complex index of refraction of the dispersive medium occupying the half-space $z>0$ with complex-valued dielectric permittivity $\epsilon(\omega)$. For a dielectric Lorentz medium with a single-resonance frequency the complex index of refraction is given by[23]

$$n(\omega)=\left[1-\frac{b^2}{\omega^2-\omega_0^2+2i\delta\omega}\right]^{1/2} \ . \tag{1.5}$$

Here $b^2=4\pi Ne^2/m$ is the square of the plasma frequency of the medium, N is the number density of electrons of charge e and mass m that are harmonically bound with the undamped resonance frequency ω_0, and δ is the associated phenomenological damping constant. The Lorentz model is used here because it is a causal model,[23] the complex index of refraction (1.5) satisfying the Kramers-Kronig relations.

If $f(t)=0$ for $t<0$, then the integral expression (1.1) is taken to be a Laplace representation in which the contour of integration C in the complex ω plane is the straight line $\omega=\omega'+ia$ with a being a fixed positive constant that is greater than the abscissa of absolute convergence[24] for the function $f(t)$ and where $\omega'\equiv\mathrm{Re}(\omega)$ ranges from negative to positive infinity. The complex phase function $\phi(\omega,\theta)$ appearing in Eq. (1.1) is given by

$$\begin{aligned}\phi(\omega,\theta)&=i\frac{c}{z}[\tilde{k}(\omega)z-\omega t]\\&=i\omega[n(\omega)-\theta] \ ,\end{aligned} \tag{1.6}$$

where

$$\theta=\frac{ct}{z} \tag{1.7}$$

is a dimensionless parameter that characterizes a space-time point in the field. A complete description of the analytic structure of $n(\omega)$ and $\phi(\omega,\theta)$ in the complex ω plane may be found in Ref. 5.

The uniform asymptotic description of the dynamical field evolution in the mature dispersion regime is developed here for an initial rectangular-modulated sine wave of applied signal frequency ω_c where

$$f(t)=u(t)\sin(\omega_c t) \ , \tag{1.8}$$

and where

$$u(t)=\begin{cases}0, & t<0\\1, & 0<t<T\\0, & T<t\end{cases} \tag{1.9}$$

the initial pulse duration being T. This rectangular envelope can also be represented by the difference between two unit-step-function-modulated signals that are displaced in time by T. The initial envelope spectrum is then

$$\tilde{u}(\omega)=\int_0^T e^{i\omega t}dt=\frac{e^{i\omega T}-1}{i\omega} \ , \tag{1.10}$$

and the integral representation (1.1) of the propagated signal becomes

$$\begin{aligned}A(z,t)&=\frac{1}{2\pi}\mathrm{Re}\left[i\int_{ia-\infty}^{ia+\infty}\tilde{u}(\omega-\omega_c)e^{(z/c)\phi(\omega,\theta)}d\omega\right]\\&=-\frac{1}{2\pi}\mathrm{Re}\left[\int_{ia-\infty}^{ia+\infty}\frac{1}{\omega-\omega_c}e^{(z/c)\phi(\omega,\theta)}d\omega-e^{-i\omega_c T}\int_{ia-\infty}^{ia+\infty}\frac{1}{\omega-\omega_c}e^{(z/c)\phi(\omega,\theta)+i\omega T}d\omega\right]\end{aligned} \tag{1.11}$$

for $z\geq 0$. By writing the complex phase function in the more general form

$$\phi(\omega,\theta_T)=i\omega[n(\omega)-\theta_T] \ , \tag{1.12}$$

with

$$\theta_T=\frac{c}{z}(t-T) \ , \tag{1.13}$$

the integral representation (1.11) of the field may then be written as

$$A(z,t)=-\frac{1}{2\pi}\mathrm{Re}\left[\int_{ia-\infty}^{ia+\infty}\frac{1}{\omega-\omega_c}e^{(z/c)\phi(\omega,\theta)}d\omega-e^{-i\omega_c T}\int_{ia-\infty}^{ia+\infty}\frac{1}{\omega-\omega_c}e^{(z/c)\phi(\omega,\theta_T)}d\omega\right] \tag{1.14}$$

for $z \geq 0$. Both integrals appearing in this expression are exactly the same as that obtained in the integral representation for the unit-step-function-modulated signal,[1-6] except that in the second integral the phase function is retarded in time by the initial pulse width T. One then has that

$$A(z,t)=U(z,t,0)-U(z,t,T)\ , \tag{1.15}$$

where

$$U(z,t,T)=-\frac{1}{2\pi}\mathrm{Re}\left[e^{-i\omega_c T}\times\int_{ia-\infty}^{ia+\infty}\frac{1}{\omega-\omega_c}e^{(z/c)\phi(\omega,\theta_T)}d\omega\right] \tag{1.16}$$

is the propagated plane wave field for $z \geq 0$ due to an input unit-step-function-modulated signal of fixed carrier frequency ω_c that begins to oscillate at time $t=T$ in the $z=0$ plane.

The propagated field $U(z,t,T)$ identically vanishes for all $\theta_T < 1$, as proven in Refs. 1-5. For all $\theta_T \geq 1$ the uniform asymptotic expansion of (1.16) may be expressed in the form[4-6]

$$U(z,t,T)=U_S(z,t,T)+U_B(z,t,T)+U_c(z,t,T)+R(z,\theta_T)\ . \tag{1.17}$$

An estimate of the remainder term $R(z,\theta_T)$ as $z\to\infty$ may be found in Ref. 6. This representation is uniformly valid for all $\theta_T \geq 1$ provided that ω_c is bounded away from infinity. An important feature of Eq. (1.17) is that the asymptotic behavior of the propagated plane-wave field $U(z,t,T)$ is expressed as the sum of three terms which are essentially uncoupled so that they can be treated independently of one another. These three terms arise from the asymptotic contributions of the saddle points of $\phi(\omega,\theta_T)$ and from the simple pole contribution at $\omega=\omega_c$. For a single-resonance Lorentz medium the complex phase function ϕ possesses two sets of saddle points in the complex ω plane; one set resides in the region removed from the origin, called the distant saddle points, and the other set resides in the region about the origin, called the near saddle points. The representation (1.17) is obtained by expressing the integral representation (1.16) of $U(z,t,T)$ in terms of an integral $I(z,\theta_T)$ with the same integrand but with a new contour of integration $P(\theta_T)$ to which the original contour of integration may be deformed and which is divisible into a sum of subpaths, each of which is an Olver-type path[25] with respect to one of the saddle points of $\phi(\omega,\theta_T)$, as described in Ref. 5. An example of such a path $P(\theta)$ and its component subpaths is illustrated in Fig. 1.

The dynamic behavior of the field component $U_S(z,t,T)$ is determined by the dynamical evolution of the distant saddle points $\mathrm{SP}_D^{\pm}$ of the complex phase function $\phi(\omega,\theta_T)$, whose locations are given by[4,5]

$$\omega_{\mathrm{SP}_D}^{\pm}(\theta_T)\cong\pm\xi(\theta_T)-\delta i[1+\eta(\theta_T)]\ , \tag{1.18}$$

with

$$\xi(\theta_T)=\left[\omega_0^2-\delta^2+\frac{b^2\theta_T^2}{\theta_T^2-1}\right]^{1/2}\ , \tag{1.19a}$$

$$\eta(\theta_T)=\frac{\delta^2/27+b^2/(\theta_T^2-1)}{\xi^2(\theta_T)}\ , \tag{1.19b}$$

and the value of the integrand of (1.16) at those saddle points. At $\theta_T=1$ the distant saddle points are at $\pm\infty-2i\delta$ and as $\theta_T\to\infty$ they approach the outer branch points

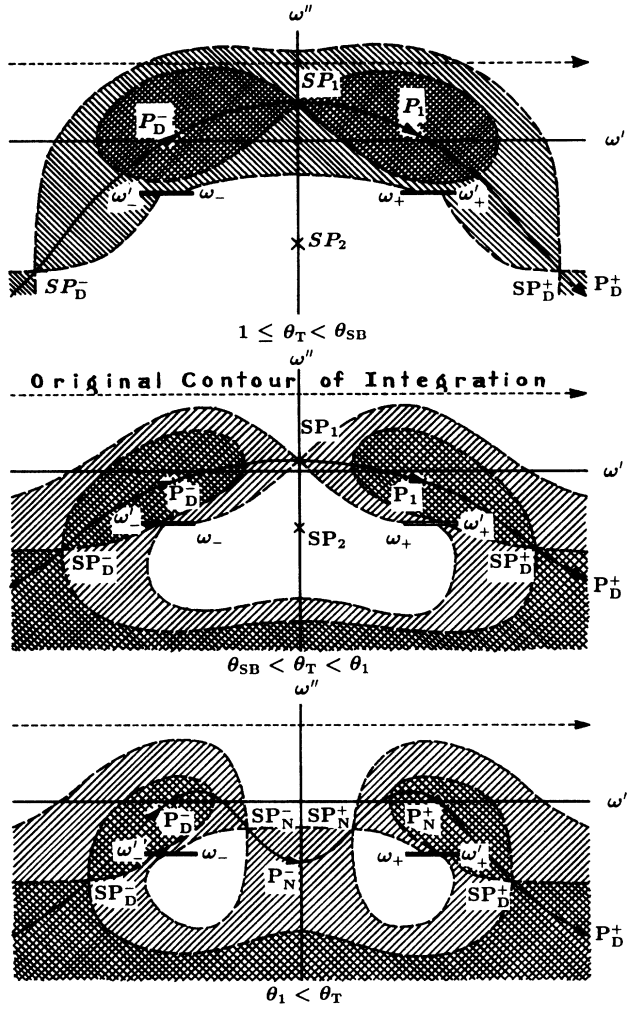

FIG. 1. The deformed contour of integration $P(\theta_T)$ through the relevant saddle points of $\phi(\omega,\theta_T)$. The dashed contours indicate the isotimic contours of $X(\omega,\theta_T)=\mathrm{Re}[\phi(\omega,\theta_T)]$ through the saddle points, and the shaded areas indicate the regions of the complex ω plane wherein $X(\omega,\theta_T)$ is less than that at the relevant saddle point. The subpaths $P_D^{\pm}(\theta_T)$ and $P_N^{\pm}(\theta_T)$ are Olver-type paths with respect to the saddle points $SP_D^{\pm}$ and $SP_N^{\pm}$, respectively, and the subpath $P_1(\theta)$ is an Olver-type path with respect to the upper saddle point SP_1 for $1 \leq \theta_T \leq \theta_1$.

$$\omega_{\pm}'=\pm(\omega_1^2-\delta^2)^{1/2}-\delta i \tag{1.20}$$

of the complex phase function $\phi(\omega,\theta_T)=X(\omega,\theta_T)+iY(\omega,\theta_T)$, as illustrated in Fig. 2, where

$$\omega_1=(\omega_0^2+b^2)^{1/2} . \tag{1.21}$$

The θ_T dependences of the complex phase function and its second derivative with respect to ω at the distant first-order saddle points are found to be given by[5]

$$\phi(\omega_{\mathrm{SP}_D}^{\pm},\theta_T)\cong -\delta\left[[1+\eta(\theta_T)](\theta_T-1)+\frac{b^2[1-\eta(\theta_T)]/2}{\xi^2(\theta_T)+\delta^2[1-\eta(\theta_T)]^2}\right]\pm i\xi(\theta_T)\left[\theta_T-1+\frac{b^2/2}{\xi^2(\theta_T)+\delta^2[1-\eta(\theta_T)]^2}\right] , \tag{1.22a}$$

$$\phi^{(2)}(\omega_{\mathrm{SP}_D}^{\pm},\theta_T)\cong -i\frac{b^2}{\{\pm\xi(\theta_T)+\delta i[1-\eta(\theta_T)]\}^3} . \tag{1.22b}$$

These approximations provide an accurate description to the actual distant saddle-point behavior for all $\theta_T\geq 1$ and reduce to the expressions given by Brillouin[2,3] as $\theta_T\rightarrow 1+$. The uniform asymptotic contribution to the field (1.16) due to this pair of distant saddle points, which gives the Sommerfeld precursor field $U_S(z,t,T)$, is presented in Sec. II.

The dynamic behavior of the field component $U_B(z,t,T)$ is determined by the dynamical evolution of the near saddle points $\mathrm{SP}_1=\mathrm{SP}_N^+$ for $1\leq\theta_T\leq\theta_1$ and $\mathrm{SP}_N^{\pm}$ for $\theta_T>\theta_1$ as well as the value of the integrand at these saddle points. The near saddle-point locations are given by[5]

$$\omega_{\mathrm{SP}_N}^{\pm}(\theta_T)\cong\begin{cases} i[\pm|\psi(\theta_T)|-\frac{2}{3}\delta\zeta(\theta_T)], & 1\leq\theta_T<\theta_1 \\ -\dfrac{2\delta}{3\alpha}i, & \theta_T=\theta_1 \\ \pm\psi(\theta)-\frac{2}{3}i\delta\zeta(\theta), & \theta_T>\theta_1 \end{cases} \tag{1.23}$$

with

$$\psi(\theta_T)=\left[\frac{\omega_0^2(\theta_T^2-\theta_0^2)}{\theta_T^2-\theta_0^2+3\alpha b^2/\omega_0^2}-\delta^2\left[\frac{\theta_T^2-\theta_0^2+2b^2/\omega_0^2}{\theta_T^2-\theta_0^2+3\alpha b^2/\omega_0^2}\right]^2\right]^{1/2} , \tag{1.24a}$$

$$\zeta(\theta_T)=\frac{3}{2}\frac{\theta_T^2-\theta_0^2+2b^2/\omega_0^2}{\theta_T^2-\theta_0^2+3\alpha b^2/\omega_0^2} , \tag{1.24b}$$

where the parameter α is given by

$$\alpha=1-\frac{\delta^2}{3\omega_0^2\omega_1^2}(4\omega_1^2+b^2) . \tag{1.25}$$

Here

$$\theta_0=n(0)=\left[1+\frac{b^2}{\omega_0^2}\right]^{1/2} , \tag{1.26}$$

$$\theta_1\cong\theta_0+\frac{2\delta^2b^2}{\theta_0\omega_0^2(3\alpha\omega_0^2-4\delta^2)} . \tag{1.27}$$

For $1\leq\theta_T<\theta_1$ the two near first-order saddle points are along the imaginary axis symmetrically situated about the point $-(2\delta/3\alpha)i$, as illustrated in Fig. 3; at $\theta_T=\theta_1$ these two saddle points have coalesced into a single second-order saddle point, as illustrated in Fig. 4; and for $\theta_T>\theta_1$ they are symmetrically situated about the imaginary axis in the lower-half plane and approach the inner branch points

$$\omega_{\pm}=\pm(\omega_0^2-\delta^2)^{1/2}-\delta i , \tag{1.28}$$

as $\theta_T\rightarrow\infty$, as illustrated in Fig. 5. The θ_T dependences of the complex phase function and its next nonvanishing higher-order derivative with respect to ω at the appropriate near saddle points are then found to be given by[5]

$$\phi(\omega_{\mathrm{SP}_1},\theta_T)\cong\tfrac{1}{3}[2\delta\zeta(\theta_T)-3|\psi(\theta_T)|](\theta_0-\theta_T)+\frac{b^2}{54\theta_0\omega_0^4}[2\delta\zeta(\theta_T)-3|\psi(\theta_T)|]^2\times\{2\delta[3-\alpha\zeta(\theta_T)]+3\alpha|\psi(\theta_T)|\} , \tag{1.29a}$$

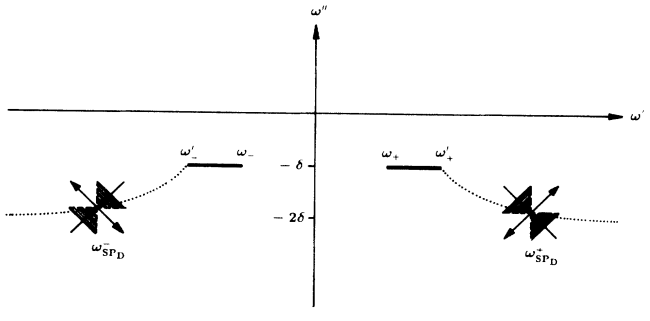

FIG. 2. The dynamical evolution of the distant saddle points $\mathrm{SP}_D^{\pm}$ in the complex ω plane. The dotted curves indicate the trajectories followed by the saddle points as θ_T varies. The arrows indicate the direction of ascent along the lines of steepest descent and ascent through the saddle points. The shaded areas indicate the regions in a neighborhood about the saddle points where in the inequality $X(\omega,\theta_T)<X(\omega_{\mathrm{SP}_D}^{\pm},\theta_T)$ is satisfied and in which the path of descent from each saddle point lies.

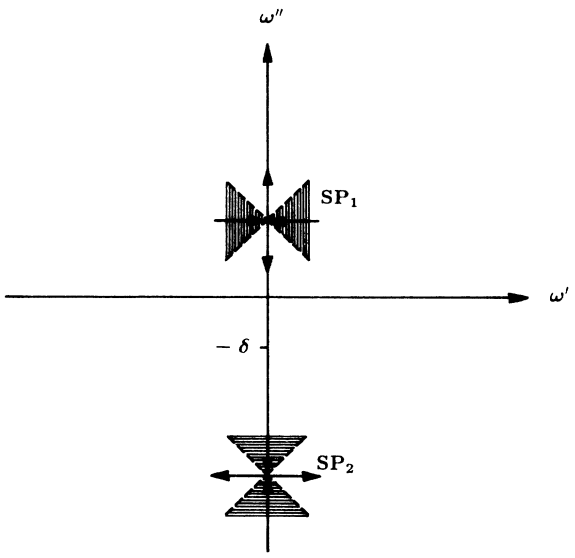

FIG. 3. The dynamical evolution of the near saddle points SP_1 and SP_2 in the complex ω plane for $1 \leq \theta_T < \theta_1$. As θ_T increases over this range the two saddle points steadily approach each other along the imaginary axis. The arrows indicate the direction of ascent along the lines of steepest descent and ascent through the saddle points.

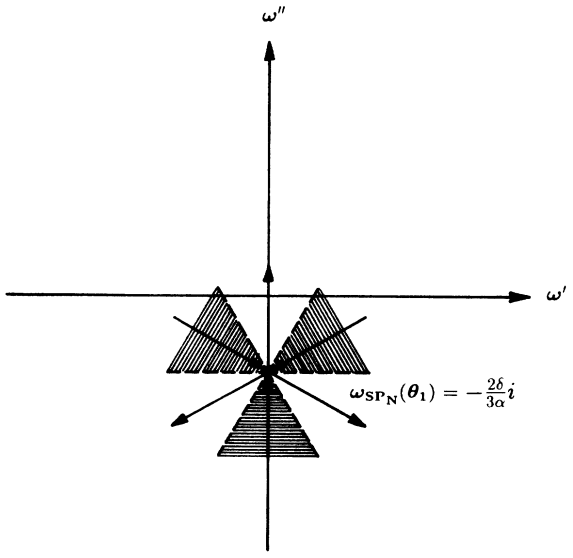

FIG. 4. The two near saddle points have coalesced into a single saddle point SP_N of second-order at $\theta_T = \theta_1$. The arrows indicate the direction of ascent along the lines of steepest descent and ascent through the saddle point.

$$\phi^{(2)}(\omega_{SP_1},\theta_T) \cong -\frac{b^2}{\theta_0\omega_0^4}\{2\delta[1-\alpha\zeta(\theta_T)]+3\alpha|\psi(\theta_T)|\}\ , \tag{1.29b}$$

for $1 \leq \theta_T < \theta_1$, where $\omega_{SP_1} = \omega^+_{SP_N}$ is the upper near saddle point (the lower near saddle point SP_2 does not contribute over this θ_T range),

$$\phi(\omega_{SP_N},\theta_1) \cong \frac{2\delta}{3\alpha}\left[\theta_0-\theta_1+\frac{4\delta^2b^2}{9\alpha\theta_0\omega_0^4}\right]\ , \tag{1.30a}$$

$$\phi^{(3)}(\omega_{SP_N},\theta_1) \cong 3i\frac{\alpha b^2}{\theta_0\omega_0^4}\ , \tag{1.30b}$$

for $\theta_T = \theta_1$ when the two near first-order saddle points have coalesced into a single second-order saddle point, and

$$\phi(\omega^{\pm}_{SP_N},\theta_T) \cong -\delta\left[\tfrac{2}{3}\zeta(\theta_T)(\theta_T-\theta_0)+\frac{b^2}{\theta_0\omega_0^4}\{[1-\alpha\zeta(\theta_T)]\psi^2(\theta_T)+\tfrac{4}{9}\delta^2\zeta^2(\theta_T)[\tfrac{1}{3}\alpha\zeta(\theta_T)-1]\}\right]$$

$$\pm i\psi(\theta_T)\left[\theta_0-\theta_T+\frac{b^2}{2\theta_0\omega_0^4}\{\tfrac{4}{3}\delta^2\zeta(\theta_T)[2-\alpha\zeta(\theta_T)]+\alpha\psi^2(\theta_T)\}\right]\ , \tag{1.31a}$$

$$\phi^{(2)}(\omega^{\pm}_{SP_N},\theta_T) \cong \frac{b^2}{\theta_0\omega_0^4}\{2\delta[\alpha\zeta(\theta_T)-1]\pm 3i\alpha\psi(\theta_T)\}\ , \tag{1.31b}$$

for $\theta_T > \theta_1$. These expressions provide an accurate description to the actual behavior at the near saddle points for all $\theta_T \geq 1$ and reduce to the approximations given by Brillouin[2,3] as $\theta \to \theta_0$. The uniform asymptotic contribution to the field (1.16) due to the near saddle points, which gives the Brillouin precursor field $U_B(z,t,T)$, is presented in Sec. III.

The near saddle point SP_1 is dominated by the distant saddle points $SP^{\pm}_D$ for $\theta_T < \theta_{SB}$, is of equal dominance with the distant saddle points at $\theta = \theta_{SB}$, remains dominant over the distant saddle points for $\theta_{SB} < \theta_T \leq \theta_1$, and for all $\theta_T > \theta_1$ the pair of near saddle points $SP^{\pm}_N$ remains dominant over the two distant saddle points $SP^{\pm}_D$, where[4,5]

$$\theta_{SB} \cong \theta_0 - \frac{4\delta^2b^2}{3\theta_0\omega_0^4} - \left[\frac{27\delta^2b^2(\theta_0-1)^2}{4\theta_0\omega_0^4}\right]^{1/3}\left\{\left[\left[1+\frac{\delta^2b^2}{27\theta_0(\theta_0-1)\omega_0^4}\right]^{1/2}+1\right]^{1/3} - \left[\left[1+\frac{\delta^2b^2}{27\theta_0(\theta_0-1)\omega_0^4}\right]^{1/2}-1\right]^{1/3}\right\} \tag{1.32}$$

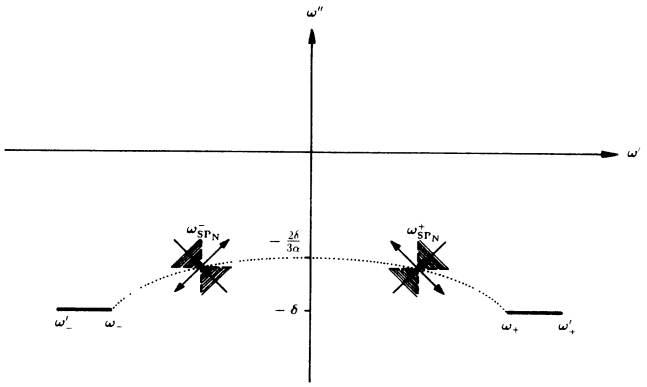

FIG. 5. The dynamical evolution of the near saddle points $SP_N^{\pm}$ in the complex ω plane for $\theta_T > \theta_1$. The dotted curves indicate the trajectories followed by the saddle points as θ_T varies. The arrows indicate the direction of ascent along the lines of steepest descent and ascent through the saddle points. The shaded areas indicate the regions in a neighborhood about the saddle points wherein the inequality $X(\omega,\theta_T) < X(\omega_{SP_n}^{\pm},\theta_T)$ is satisfied and in which the path of descent from each saddle point lies.

to a good degree of accuracy.

The dynamic behavior of the field component $U_c(z,t,T)$ is determined both by the poles of the spectral function $\tilde{u}(\omega-\omega_c)$ and by the dynamical evolution of the saddle points that interact with these poles. The contribution $U_c(z,t,T)$ is nonzero only if $\tilde{u}(\omega-\omega_c)$ has poles. If the envelope function $u(t)$ of the field on the plane $z=0$ is bounded for all time t, then $\tilde{u}(\omega-\omega_c)$ can have poles only if $u(t)$ does not tend to zero too fast as $t\to\infty$. Hence the implication of nonzero $U_c(z,t,T)$ is that the field $U(0,t,T)$ oscillates with angular frequency ω_c for $t > T$ on the plane $z=0$ and will tend to do the same at values $z > 0$ for sufficiently large t. As a result, the contribution $U_c(z,t,T)$ describes the dynamic evolution of the propagated signal that is oscillating with fixed angular frequency ω_c. This contribution is asymptotically negligible during most of the precursor field evolution, provided that $\omega_c < \omega_{SB}$, where[4,5]

$$\omega_{SB} \cong \xi(\theta_{SB}) \approx \omega_0 \left[2 + \frac{b^2}{\omega_0^2} + \frac{5\delta^2}{3\omega_0^2} \right]^{1/2} . \tag{1.33}$$

When $\omega_c > \omega_{SB}$ the distant saddle point SP_D^+ passes in the vicinity of the pole when it is the dominant saddle point and the associated pole contribution will first become dominant over the Sommerfeld precursor field at a value $\theta_T = \theta_{c1}$ between 1 and θ_{SB}. The Brillouin precursor field then becomes dominant over this pole contribution at a value $\theta_T = \theta_{c2}$ between θ_{SB} and θ_0. This pole contribution then becomes dominant over the second precursor field at a value $\theta_T = \theta_c > \theta_0$ and remains dominant for all larger values of θ_T. In this situation the contribution $U_c(z,t,T)$ describes the dynamical evolution of the signal oscillating at ω_c that is asymptotically dominant over a short space-time interval between the individual Sommerfeld and Brillouin precursor field evolutions and is again asymptotically dominant following the Brillouin precursor field evolution.[4,5] The signal evolution over the interval $\theta_{c1} < \theta_T < \theta_{c2}$ is called the prepulse and the signal evolution for $\theta_T > \theta_c$ is called the main signal for the input unit-step-function modulated field.

For most values of θ_T only one of the field components $U_S(z,t,T)$, $U_B(z,t,T)$, and $U_c(z,t,T)$ appearing in Eq. (1.17) is important at a time. There are short intervals of θ_T, however, during which two or more of these terms are significant for fixed values of the propagation distance z. These intervals mark the transition periods when the propagated field $U(z,t,T)$ is changing its character from one form to another and the presence of both terms in the expression leads to a continuous transition in the behavior of the field.[6] As a consequence, Eq. (1.17) displays the entire evolution of the propagated field $U(z,t,T)$ through its various components in a continuous manner.

From Eqs. (1.15) and (1.17) it is seen that the uniform asymptotic expansion of the propagated field due to an input rectangular-modulated signal of carrier frequency ω_c is given by

$$A(z,t) \sim U_S(z,t,0) + U_B(z,t,0) + U_c(z,t,0) - U_S(z,t,T) - U_B(z,t,T) - U_c(z,t,T) . \tag{1.34}$$

It is then seen that for a sufficiently long initial pulse width T and/or a sufficiently short propagation distance z such that $(c/z)T > \theta_c$, the first and second precursor fields associated with the leading edge $U(z,t,0)$ of the pulse will completely evolve prior to the arrival of the precursor fields associated with the trailing edge $U(z,t,T)$ of the pulse. Indeed, the trailing edge precursors will arrive only after the main signal of the leading edge has arrived and is evolving. Hence, when this condition prevails the interference between the precursor fields of the leading and trailing edges of the pulse is minimal and the pulse distortion is also minimal. For shorter initial pulse widths T or longer propagation distances z such that $\theta_c > (c/z)T > \theta_{SB}$, the first precursor field $U_S(z,t,0)$ associated with the leading edge of the pulse will still evolve undisturbed, but during the evolution of the second precursor field $U_B(z,t,0)$ the arrival and evolution of the precursor fields associated with the trailing edge of the pulse will occur. Hence, when this condition prevails there will be interference between the Brillouin precursor of the leading edge and the Sommerfeld precursor of the trailing edge of the pulse and the resultant pulse distortion is found to be moderate. Finally, for even shorter initial pulse widths T or longer propagation distances z such that $1 < (c/z)T \leq \theta_{SB}$ there will be a complete overlap of these two sets of precursor fields and the resultant pulse distortion is found to be severe.

This qualitative description of rectangular pulse distortion in a causally dispersive medium, which is based upon the uniform asymptotic description of the difference in

the fields due to two time-displaced unit-step-function-modulated signals, as embodied in Eq. (1.34), is given quantitative meaning in the remainder of this paper. In Secs. II–IV the uniform asymptotic expressions for the general field components $U_S(z,t,T)$, $U_B(z,t,T)$, and $U_c(z,t,T)$ are presented based upon the detailed derivations of their $T=0$ counterparts given in Ref. 6. The resultant uniform asymptotic description of rectangular pulse dispersion is then given in Sec. VI following a description of the signal arrival and signal velocity in Sec. V. The accuracy of this analytical description in the mature dispersion regime is demonstrated through a detailed comparison with purely numerical calculations.

II. UNIFORM ASYMPTOTIC DESCRIPTION OF THE SOMMERFELD PRECURSOR FIELD $U_S(z,t,T)$

The uniform asymptotic behavior of the propagated plane-wave field (1.16) as $z\to\infty$ that is due to the pair of distant saddle points (1.18) yields the first or Sommerfeld precursor of the field. Since the integral representation (1.16) for $U(z,t,T)$ is of exactly the same form as that for $U(z,t,0)$, with the exception that it is retarded in θ by the amount $-(c/z)T$ and is multiplied by the additional phase factor $\exp(-i\omega_c T)$, the first precursor field associated with this integral may easily be constructed from the analysis of Sec. III of Ref. 6, with the result

$$U_S(z,t,T)\sim\frac{1}{2b}\xi(\theta_T)\left[\theta_T-1+\frac{b^2/2}{\xi^2(\theta_T)+\delta^2[1-\eta(\theta_T)]^2}\right]^{1/2}$$
$$\times\exp\left[-\delta\frac{z}{c}\left[[1+\eta(\theta_T)](\theta_T-1)+\frac{[1-\eta(\theta_T)]b^2/2}{\xi^2(\theta_T)+\delta^2[1-\eta(\theta_T)]^2}\right]\right]$$
$$\times\left[\left[\frac{-\lambda_1^-(\theta_T)\cos(\omega_c T)+\lambda_2^-(\theta_T)\sin(\omega_c T)}{\lambda_3^-(\theta_T)}+\frac{\lambda_1^+(\theta_T)\cos(\omega_c T)+\lambda_2^+(\theta_T)\sin(\omega_c T)}{\lambda_3^+(\theta_T)}\right]J_0\left[\frac{z}{c}\xi(\theta_T)\varphi(\theta_T)\right]\right.$$
$$\left.+\left[\frac{\lambda_1^-(\theta_T)\sin(\omega_c T)+\lambda_2^-(\theta_T)\cos(\omega_c T)}{\lambda_3^-(\theta_T)}+\frac{\lambda_1^+(\theta_T)\sin(\omega_c T)-\lambda_2^+(\theta_T)\cos(\omega_c T)}{\lambda_3^+(\theta_T)}\right]J_1\left[\frac{z}{c}\xi(\theta_T)\varphi(\theta_T)\right]\right] \tag{2.1}$$

as $z\to\infty$ uniformly for all $\theta_T\geq 1$. Here J_ν denotes the Bessel function of the first kind of integer order ν, and

$$\lambda_1^\pm(\theta_T)=\tfrac{1}{2}\delta\{\xi(\theta_T)[5-\eta(\theta_T)]\pm 3\omega_c[1-\eta(\theta_T)]\}\ , \tag{2.2}$$

$$\lambda_2^\pm(\theta_T)=\xi(\theta_T)[\xi(\theta_T)\pm\omega_c]-\tfrac{3}{2}\delta^2[1-\eta^2(\theta_T)]\ , \tag{2.3}$$

$$\lambda_3^\pm(\theta_T)=[\xi(\theta_T)\pm\omega_c]^2+\delta^2[1+\eta(\theta_T)]^2\ , \tag{2.4}$$

$$\varphi(\theta_T)=\theta_T-1+\frac{b^2/2}{\xi^2(\theta_T)+\delta^2[1-\eta(\theta_T)]^2}\ . \tag{2.5}$$

It is seen from Eq. (2.1) that $U_S(z,t,T)$ vanishes at $\theta_T=1$, but is nonzero for $\theta_T=1+\epsilon$, where $\epsilon>0$ can be arbitrarily small. Consequently, the front of the Sommerfeld precursor travels with the velocity of light c in vacuum. For values of $\theta_T>1$ bounded away from unity the two Bessel functions appearing in Eq. (2.1) may be replaced by their large argument asymptotic approximations, with the result

$$U_S(z,t,T)\sim-\left[\frac{c\xi(\theta_T)}{2\pi z}\right]^{1/2}\frac{1}{b}\exp\left[-\delta\frac{z}{c}\left[[1+\eta(\theta_T)](\theta_T-1)+\frac{[1-\eta(\theta_T)]b^2/2}{\xi^2(\theta_T)+\delta^2[1-\eta(\theta_T)]^2}\right]\right]$$
$$\times\left[\frac{\lambda_2^-(\theta_T)}{\lambda_3^-(\theta_T)}\cos\left[\frac{z}{c}\xi(\theta_T)\varphi(\theta_T)+\frac{\pi}{4}+\omega_c T\right]-\frac{\lambda_2^+(\theta_T)}{\lambda_3^+(\theta_T)}\cos\left[\frac{z}{c}\xi(\theta_T)\varphi(\theta_T)+\frac{\pi}{4}-\omega_c T\right]\right.$$
$$\left.+\frac{\lambda_1^-(\theta_T)}{\lambda_3^-(\theta_T)}\sin\left[\frac{z}{c}\xi(\theta_T)\varphi(\theta_T)+\frac{\pi}{4}+\omega_c T\right]-\frac{\lambda_1^+(\theta_T)}{\lambda_3^+(\theta_T)}\sin\left[\frac{z}{c}\xi(\theta_T)\varphi(\theta_T)+\frac{\pi}{4}-\omega_c T\right]\right] \tag{2.6}$$

as $z \to \infty$ with $\theta_T \geq 1+\epsilon$ with $\epsilon > 0$. Notice that Eq. (2.1) reduces to the uniform asymptotic expression for the Sommerfeld precursor field $U_S(z,t,0)$ due to a unit-step-function-modulated signal given in Ref. 6 when $\omega_c T = 2n\pi$, $n = 0,1,2,3,\ldots$, while Eq. (2.6) reduces to the nonuniform asymptotic expression for $U_S(z,t,0)$ given in Ref. 5 under the same condition.

The dynamical evolution with θ_T of the Sommerfeld precursor field structure, as given by the uniform asymptotic expansion (2.1), is illustrated in Fig. 6 at a fixed propagation distance of $z = 1\times 10^{-3}$ cm with applied signal frequency $\omega_c = 1\times 10^{16}$/sec. The Lorentz medium parameters used here and throughout this paper are $\omega_0 = 4\times 10^{16}$/sec, $b^2 = 20\times 10^{32}$/sec^2, $\delta = 0.28\times 10^{16}$/sec, which corresponds to a highly dispersive and absorptive medium. Notice the rapid rise in the Sommerfeld precursor field amplitude to a maximum value soon after $\theta_T = 1$, which is then followed by a slow decay in the amplitude as the medium attenuation increases because of the decrease in the oscillation frequency of the field. The instantaneous angular frequency of oscillation of the Sommerfeld precursor field is found to be given by[4,5]

$$\omega_s = \frac{d}{dt}\left[\frac{z}{c}\xi(\theta_T)\left[\theta_T - 1 + \frac{b^2/2}{\xi^2(\theta_T)+\delta^2[1-\eta(\theta_T)]^2}\right]\right]$$

$$= \xi(\theta_T) + \frac{b^2\theta_T}{2\xi(\theta_T)(\theta_T^2-1)^2}\left[b^2\frac{\xi^2(\theta_T)-5\delta^2[1-\eta(\theta_T)]^2}{\{\xi^2(\theta_T)+\delta^2[1-\eta(\theta_T)]^2\}^2} - 2(\theta_T-1)\right] \tag{2.7a}$$

$$\cong \xi(\theta_T)\ . \tag{2.7b}$$

The approximation given in part (b) of this equation is obtained from part (a) in the small $\theta_T - 1$ limit. It is found from numerical calculations of the precursor field structure[11] that this approximation yields a very accurate description of the instantaneous angular frequency of oscillation of the Sommerfeld precursor and that this quantity is also given to a high degree of accuracy by the frequency of oscillation that is determined from the energy transport velocity in the dispersive medium.[7] The dynamical evolution of the instantaneous angular frequency of oscillation $\omega_s \simeq \xi(\theta_T) = \mathrm{Re}[\omega^+_{\mathrm{SP}_D}(\theta_T)]$ is illustrated in Fig. 7 for the above set of medium parameters. Notice that ω_s rapidly decreases from its infinite value at

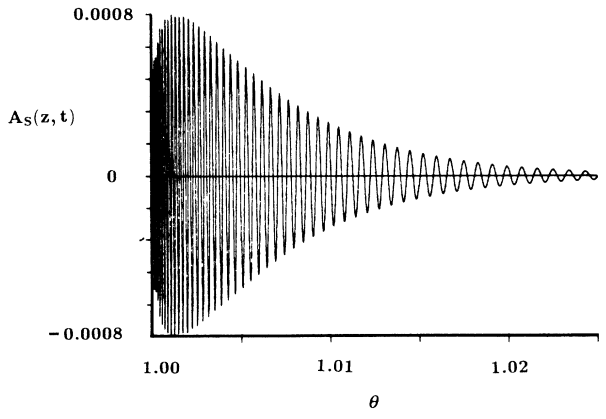

FIG. 6. Uniform asymptotic behavior of the Sommerfeld precursor field $U_S(z,t,T)$ for an input unit-step-function-modulated signal at $t = T$ with carrier frequency $\omega_c = 1\times 10^{-3}$ cm in a highly absorptive and dispersive medium.

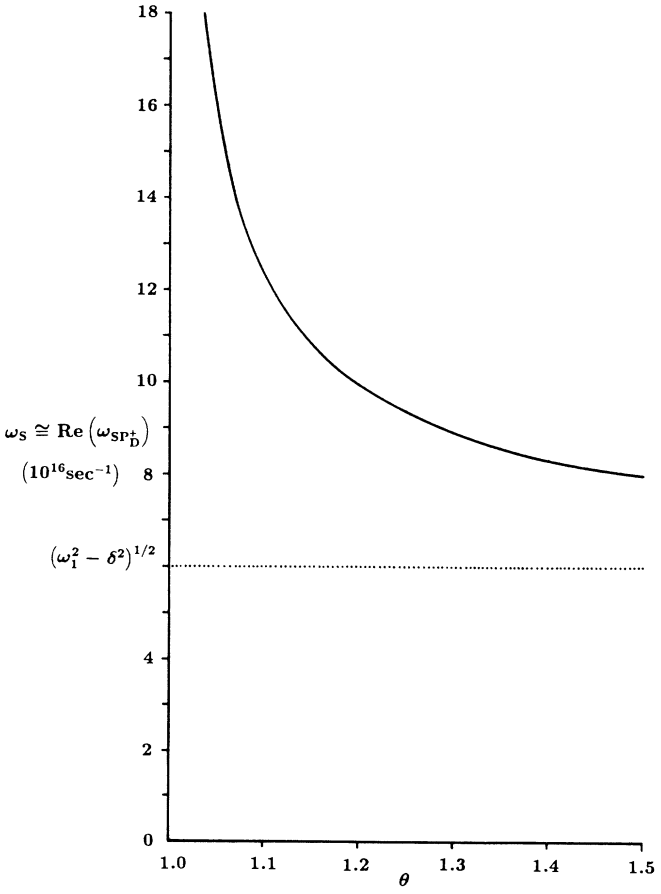

FIG. 7. The evolution of the instantaneous angular frequency of oscillation $\omega_s \cong \mathrm{Re}(\omega^+_{\mathrm{SP}_D})$ of the Sommerfeld precursor field.

$\theta_T=1$ and monotonically approaches the limiting value $(\omega_1^2-\delta^2)^{1/2}$ as $\theta_T\to\infty$.

III. UNIFORM ASYMPTOTIC DESCRIPTION OF THE BRILLOUIN PRECURSOR FIELD $U_B(z,t,T)$

The uniform asymptotic behavior of the propagated plane-wave field (1.16) as $z\to\infty$ that is due to the upper near saddle point SP_N^+ for $1<\theta_T\le\theta_1$ and the symmetric pair of near saddle points $\mathrm{SP}_N^\pm$ for $\theta_T\ge\theta_1$, whose locations are given in Eq. (1.23), yields the second or Brillouin precursor field. Since the integral representation (1.16) for $U(z,t,T)$ is given by $\exp(-i\omega_c T)U(z,t,0)$ when $U(z,t,0)$ is retarded in θ by the amount $-c/zT$, then the second precursor field associated with this integral may be readily constructed from the analysis of Sec. IV of Ref. 6. For $1<\theta_T\le\theta_1$ the uniform asymptotic description is

$$
\begin{aligned}
U_B(z,t,T)\sim\frac{\omega_0^2}{2b}\left[\frac{c}{z}\right]^{1/3}e^{(z/c)\alpha_0(\theta_T)}\Bigg\{&\omega_c\cos(\omega_c T)\Bigg[\left[\frac{\beta_3^+(\theta_T)}{\beta_1^-(\theta_T)}+\frac{\beta_3^-(\theta_T)}{\beta_1^+(\theta_T)}\right]|\alpha_1(\theta_T)|^{1/4}\mathrm{Ai}\left[|\alpha_1(\theta_T)|\left[\frac{z}{c}\right]^{2/3}\right]\\
&-\left[\frac{\beta_3^+(\theta_T)}{\beta_1^-(\theta_T)}-\frac{\beta_3^-(\theta_T)}{\beta_1^+(\theta_T)}\right]\frac{(c/z)^{1/3}}{|\alpha_1(\theta_T)|^{1/4}}\mathrm{Ai}^{(1)}\left[|\alpha_1(\theta_T)|\left[\frac{z}{c}\right]^{2/3}\right]\Bigg]\\
&+\sin(\omega_c T)\Bigg[\left[\frac{\beta_2^-(\theta_T)}{\beta_1^-(\theta_T)}\beta_3^+(\theta_T)-\frac{\beta_2^+(\theta_T)}{\beta_1^+(\theta_T)}\beta_3^-(\theta_T)\right]|\alpha_1(\theta_T)|^{1/4}\\
&\times\mathrm{Ai}\left[|\alpha_1(\theta_T)|\left[\frac{z}{c}\right]^{2/3}\right]-\left[\frac{\beta_2^-(\theta_T)}{\beta_1^-(\theta_T)}\beta_3^+(\theta_T)+\frac{\beta_2^+(\theta_T)}{\beta_1^+(\theta_T)}\beta_3^-(\theta_T)\right]\\
&\times\frac{(c/z)^{1/3}}{|\alpha_1(\theta_T)|^{1/4}}\mathrm{Ai}^{(1)}\left[|\alpha_1(\theta_T)|\left[\frac{z}{c}\right]^{2/3}\right]\Bigg]\Bigg\}
\end{aligned}
\tag{3.1}
$$

as $z\to\infty$ for all $1<\theta_T\le\theta_1$. Here Ai and $\mathrm{Ai}^{(1)}$ denote the Airy function and its first derivative, respectively, and where

$$\beta_1^\pm(\theta_T)=\omega_c^2+[|\psi(\theta_T)|\pm\tfrac{2}{3}\delta\zeta(\theta_T)]^2\,, \tag{3.2}$$

$$\beta_2^\pm(\theta_T)=|\psi(\theta_T)|\pm\tfrac{2}{3}\delta\zeta(\theta_T)\,, \tag{3.3}$$

$$\beta_3^\pm(\theta_T)=\left[\frac{2\theta_0}{3\alpha|\psi(\theta_T)|\pm2\delta[1-\alpha\zeta(\theta_T)]}\right]^{1/2}, \tag{3.4}$$

and

$$\alpha_0(\theta_T)=-\tfrac{2}{3}\delta\zeta(\theta_T)(\theta_T-\theta_0)-\frac{\delta b^2}{\theta_0\omega_0^4}\{|\psi(\theta_T)|^2[\alpha\zeta(\theta_T)-1]+\tfrac{4}{9}\delta^2\zeta^2(\theta_T)[\tfrac{1}{3}\alpha\zeta(\theta_T)-1]\}\,, \tag{3.5}$$

$$|\alpha_1(\theta_T)|=\left|\psi(\theta_T)\left[\tfrac{3}{2}(\theta_T-\theta_0)+\frac{b^2}{\theta_0\omega_0^4}[\tfrac{3}{4}\alpha|\psi(\theta_T)|^2+\alpha\delta^2\zeta^2(\theta_T)-2\delta^2\zeta(\theta_T)]\right]\right|^{2/3} \tag{3.6}$$

for $1<\theta_T\le\theta_1$. The uniform asymptotic description of the Brillouin precursor field for $\theta_T\ge\theta_1$ is given by

$$
\begin{aligned}
U_B(z,t,T)\sim-\frac{\omega_0^2}{b}&\left[\frac{\theta_0}{6\alpha\psi(\theta_T)}\right]^{1/2}e^{(z/c)\alpha_0(\theta_T)}\\
\times\Bigg\{&\cos(\omega_c T)\left[\tfrac{2}{3}\delta\zeta(\theta_T)|\alpha_1(\theta_T)|^{1/4}\left[\frac{1}{\beta_4^+(\theta_T)}-\frac{1}{\beta_4^-(\theta_T)}\right]\mathrm{Ai}\left[-|\alpha_1(\theta_T)|\left[\frac{z}{c}\right]^{2/3}\right]\right.\\
&\left.-\left[\frac{\psi(\theta_T)-\omega_c}{\beta_4^-(\theta_T)}-\frac{\psi(\theta_T)+\omega_c}{\beta_4^+(\theta_T)}\right]\frac{(c/z)^{1/3}}{|\alpha_1(\theta_T)|^{1/4}}\mathrm{Ai}^{(1)}\left[-|\alpha_1(\theta_T)|\left[\frac{z}{c}\right]^{2/3}\right]\right]\\
&+\sin(\omega_c T)\left[|\alpha_1(\theta_T)|^{1/4}\left[\frac{\psi(\theta_T)-\omega_c}{\beta_4^-(\theta_T)}+\frac{\psi(\theta_T)+\omega_c}{\beta_4^+(\theta_T)}\right]\mathrm{Ai}\left[-|\alpha_1(\theta_T)|\left[\frac{z}{c}\right]^{2/3}\right]\right.\\
&\left.-\tfrac{2}{3}\delta\zeta(\theta_T)\left[\frac{1}{\beta_4^-(\theta_T)}+\frac{1}{\beta_4^+(\theta_T)}\right]\frac{(c/z)^{1/3}}{|\alpha_1(\theta_T)|^{1/4}}\mathrm{Ai}^{(1)}\left[-|\alpha_1(\theta_T)|\left[\frac{z}{c}\right]^{2/3}\right]\right]\Bigg\}
\end{aligned}
\tag{3.7}
$$

as $z \rightarrow \infty$ uniformly for all $\theta_T \geq \theta_1$. Here

$$\beta_4^{\pm}(\theta_T)=[\psi(\theta_T)\pm\omega_c]^2+\tfrac{4}{9}\delta^2\zeta^2(\theta_T) \tag{3.8}$$

and

$$\alpha_0(\theta_T)=-\delta\left[\tfrac{2}{3}\zeta(\theta_T)(\theta_T-\theta_0)+\frac{b^2}{\theta_0\omega_0^4}\{[1-\alpha\zeta(\theta_T)]\psi^2(\theta_T)+\tfrac{4}{9}\delta^2\zeta^2(\theta_T)[\tfrac{1}{3}\alpha\zeta(\theta_T)-1]\}\right], \tag{3.9}$$

$$|\alpha_1(\theta_T)|=\left|\tfrac{3}{2}\psi(\theta_T)\left[(\theta_T-\theta_0)-\frac{b^2}{2\theta_0\omega_0^4}\{\tfrac{4}{3}\delta^2\zeta(\theta_T)[2-\alpha\zeta(\theta_T)]+\alpha\psi^2(\theta_T)\}\right]\right|^{2/3} \tag{3.10}$$

for $\theta_T \geq \theta_1$.

Taken together, Eqs. (3.1) and (3.7) provide an asymptotic description of the Brillouin precursor field $U_B(z,t,T)$ that is uniformly valid for all $\theta_T > 1$. However, for a numerical evaluation these equations are unstable and are not useful for small values of $|\theta_T-\theta_1|$, as described in Ref. 6. For that purpose they should be replaced by

$$U_B(z,t,T)\sim\frac{\omega_0}{\omega_c^2+4\delta^2/(9\alpha^2)}\left[\frac{2\theta_0\omega_0 c}{3\alpha b^2 z}\right]^{1/3}\left[\omega_c\cos(\omega_c T)-\frac{2\delta}{3\alpha}\sin(\omega_c T)\right]$$
$$\times\mathrm{Ai}\left[|\alpha_1(\theta_T)|\left[\frac{z}{c}\right]^{2/3}\right]\exp\left[\frac{2\delta z}{3\alpha c}\left[\theta_0+\frac{4\delta^2 b^2}{9\alpha\theta_0\omega_0^4}-\theta_T\right]\right] \tag{3.11}$$

for $\theta_0 \leq \theta_T \leq \theta_1$, and by

$$U_B(z,t,T)\sim\frac{\omega_0}{\omega_c^2+4\delta^2/(9\alpha^2)}\left[\frac{2\theta_0\omega_0 c}{3\alpha b^2 z}\right]^{1/3}\left[\omega_c\cos(\omega_c T)-\frac{2\delta}{3\alpha}\sin(\omega_c T)\right]$$
$$\times\mathrm{Ai}\left[-|\alpha_1(\theta_T)|\left[\frac{z}{c}\right]^{2/3}\right]\exp\left[-\frac{2\delta z}{3\alpha c}\left[\theta_T-\theta_0-\frac{4\delta^2 b^2}{9\alpha\theta_0\omega_0^4}\right]\right] \tag{3.12}$$

for $\theta_1 \leq \theta_T \leq \theta_2$, where

$$\theta_2=2\theta_1-\theta_0\ . \tag{3.13}$$

Since the argument of the Airy function and its first derivative is real and positive for $\theta_T \in (1,\theta_1]$, the Brillouin precursor field is nonoscillatory over this θ_T domain. For $\theta_T > \theta_1$ the argument of the Airy function and its first derivative is real and negative so that the Brillouin precursor is oscillatory over this final θ_T domain. The instantaneous frequency of oscillation for $\theta_T > \theta_1$ is found to be[5]

$$\omega_B=\frac{d}{dt}\left[\frac{z}{c}\psi(\theta_T)\left[\theta_T-\theta_0-\frac{b^2}{2\theta_0\omega_0^4}\{\tfrac{4}{3}\delta^2\zeta(\theta_T)[2-\alpha\zeta(\theta_T)]+\psi^2(\theta_T)\}\right]\right]$$
$$\cong\psi(\theta_T)\ . \tag{3.14}$$

The approximation given in this equation is obtained in the small $\theta_T-\theta_1$ limit. It is found from numerical calculations of the dynamical precursor field structure[11] that this approximation yields a very accurate description of the instantaneous angular frequency of oscillation of the Brillouin precursor and that this quantity is also given to a high degree of accuracy by the frequency of oscillation that is determined from the energy transport velocity in the dispersive medium.[7]

The dynamical evolution with θ_T of the Brillouin precursor field structure, as given by the uniform expansion expressed in Eqs. (3.1), (3.7), (3.11), and (3.12), is illustrated in Fig. 8 at a fixed propagation distance of $z=1\times10^{-3}$ cm with an applied signal frequency $\omega_c=1\times10^{16}$/sec. The amplitude of this precursor field is seen to grow rapidly as θ_T approaches θ_0 from below, reaches a peak amplitude near $\theta_T=\theta_0$ (at this space-time point there is no exponential attention of this field), and then decays with increasing $\theta_T > \theta_0$. At this propagation distance with an applied signal frequency $\omega_c < \omega_0$, the maximum amplitude of the Brillouin precursor is two orders of magnitude larger than the maximum amplitude attained by the Sommerfeld precursor. For $\theta_T > \theta_1$ the field oscillates with an instantaneous frequency

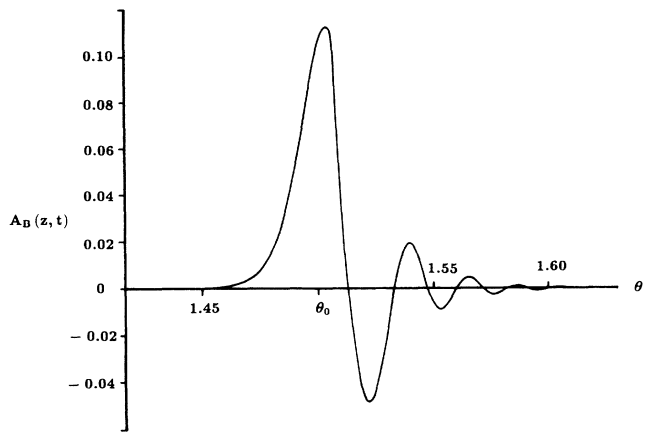

FIG. 8. Uniform asymptotic behavior of the Brillouin precursor field $U_B(z,t,T)$ for an input unit-step-function-modulated signal at $t=T$ with carrier frequency $\omega_c=1\times10^{16}$/sec at a propagation distance of $z=1\times10^{-3}$ cm in a highly absorptive and dispersive medium.

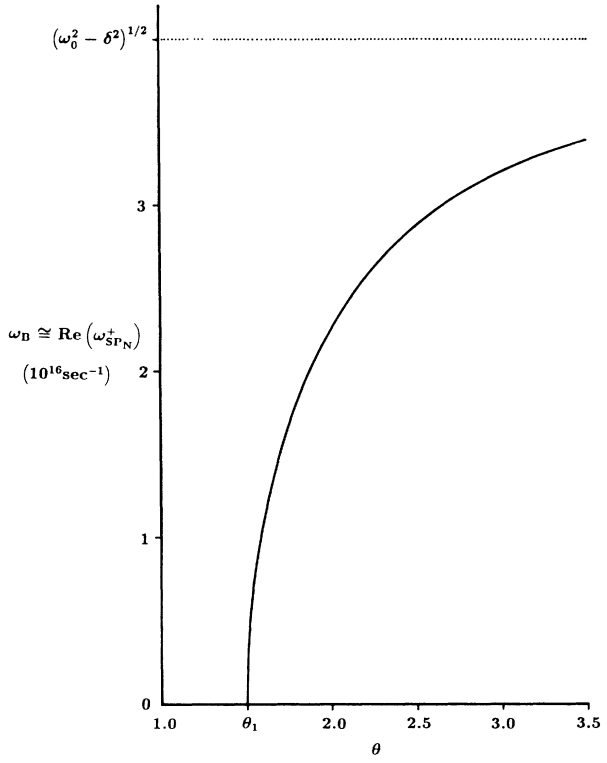

FIG. 9. The evolution of the instantaneous angular frequency of oscillation $\omega_B \cong \mathrm{Re}(\omega^+_{SP_N})$ of the Brillouin precursor field.

$\omega_B \cong \psi(\theta_T)=\mathrm{Re}[\omega^+_{SP_N}(\theta_T)]$ that monotonically increases from zero at $\theta_T=\theta_1$ and asymptotically approaches the value $\psi(\infty)=(\omega_0^2-\delta^2)^{1/2}$ from below, as illustrated in Fig. 9.

IV. UNIFORM ASYMPTOTIC DESCRIPTION OF THE FIELD $U_c(z,t,T)$ DUE TO THE POLE CONTRIBUTION

The contribution $U_c(z,t,T)$ to the asymptotic behavior of the propagated field that is due to the simple pole singularity of the spectral amplitude at $\omega=\omega_c$ is associated with the steady-state signal in the propagated field structure due to the input unit-step-function-modulated signal. Again, since the integral representation (1.16) for $U(z,t,T)$ is given by $\exp(-i\omega_c T)U(z,t,0)$ when $U(z,t,0)$ is retarded in θ by the amount $-(c/z)T$, then the uniform asymptotic description of the pole contribution in this integral may be readily constructed from the analysis of Sec. 5 of Ref. 6.

Since ω_c is real and non-negative, the complex phase behavior at the simple pole singularity is given by

$$\phi(\omega_c,\theta_T)=-\omega_c n_i(\omega_c)+i\omega_c[n_r(\omega_c)-\theta_T]\,, \tag{4.1}$$

so that the real and imaginary parts of ϕ are respectively given by

$$X(\omega_c)=-\omega_c n_i(\omega_c)\,, \tag{4.2a}$$

$$Y(\omega_c,\theta_T)=\omega_c[n_r(\omega_c)-\theta_T]\,, \tag{4.2b}$$

where $n_r(\omega_c)$ is the real part and $n_i(\omega_c)$ the imaginary part of the complex index of refraction along the negative real frequency axis. The saddle point SP_D^- and SP_N^- that are located in the left half of the complex ω plane do not interact with the pole at $\omega=\omega_c$ and, consequently, do not contribute to the asymptotic behavior of $U_c(z,t,T)$. Since the real coordinate location of the near saddle point SP_N^+ in the right half plane lies within the frequency domain from 0 to $+(\omega_0^2-\delta^2)^{1/2}$, while the real coordinate location of the distant saddle point SP_D^+ in the right half plane is greater than or equal to $+(\omega_1^2-\delta^2)^{1/2}$ for all $\theta_T\geq1$, this problem then naturally separates into three cases.

A. Signal frequencies ω_c below the absorption band: $0\leq\omega_c\leq(\omega_0^2-\delta^2)^{1/2}$

For an input signal frequency ω_c in the domain $0\leq\omega_c\leq(\omega_0^2-\delta^2)^{1/2}$, which is below the medium absorption band, it is the near saddle point in the right half of the complex ω plane that interacts with the simple pole singularity at $\omega=\omega_c$. The uniform asymptotic approximation of the pole contribution $U_c(z,t,T)$ is then given by the set of equations[6]

$$U_c(z,t,T)\sim\frac{1}{2\pi}\mathrm{Re}\left[e^{i\omega_c T}\left\{i\pi\,\mathrm{erfc}\left[i\Delta(\theta_T)\left[\frac{z}{c}\right]^{1/2}\right]e^{z/c\,\phi(\omega_c,\theta_T)}-\frac{1}{\Delta(\theta_T)}\left[\frac{\pi c}{z}\right]^{1/2}e^{(z/c)\phi(\omega_{SP},\theta_T)}\right\}\right],\quad \theta_T<\theta_s \tag{4.3a}$$

$$U_c(z,t_s',T)\sim\frac{1}{2\pi}\mathrm{Re}\left[e^{i\omega_c T}\left\{2\sqrt{\pi}e^{(z/c)\phi(\omega_{\mathrm{SP}},\theta_s)}F\left[|\Delta(\theta_s)|\left[\frac{z}{c}\right]^{1/2}\right]-\frac{1}{\Delta(\theta_s)}\left[\frac{\pi c}{z}\right]^{1/2}e^{(z/c)\phi(\omega_{\mathrm{SP}},\theta_s)}\right\}\right]$$
$$-\tfrac{1}{2}e^{-z\alpha(\omega_c)}\sin[k(\omega_c)z-\omega_c t_s'],\quad \theta_T=\theta_s=\frac{c}{z}t_s,\quad \omega_c\neq 0 \tag{4.3b}$$

$$U_c(z,t_s,T)\sim\frac{\omega_0^2}{2b}\left[\frac{\theta_0 c}{\pi\delta z}\right]^{1/2}\frac{1}{\omega_{\mathrm{SP}_1}(\theta_s)},\quad \theta_T=\theta_s=\theta_0,\quad \omega_c=0 \tag{4.3c}$$

$$U_c(z,t,T)\sim\frac{1}{2\pi}\mathrm{Re}\left[e^{i\omega_c T}\left\{-i\pi\,\mathrm{erfc}\left[-i\Delta(\theta_T)\left[\frac{z}{c}\right]^{1/2}\right]e^{(z/c)\phi(\omega_c,\theta_T)}-\frac{1}{\Delta(\theta_T)}\left[\frac{\pi c}{z}\right]^{1/2}e^{(z/c)\phi(\omega_{\mathrm{SP}},\theta_T)}\right\}\right]$$
$$-e^{-z\alpha(\omega_c)}\sin[k(\omega_c)z-\omega_c t],\quad \theta_T>\theta_s \tag{4.3d}$$

as $z\to\infty$, where $t_s'=t_s+T$. Here ω_{SP} denotes ω_{SP_1} and $\Delta(\theta_T)$ is given by

$$\Delta(\theta_T)=[\phi(\omega_{\mathrm{SP}_1},\theta_T)-\phi(\omega_c,\theta_T)]^{1/2} \tag{4.4a}$$

for $1\le\theta_T<\theta_1$, ω_{SP} denotes ω_{SP_N} and $\Delta(\theta_T)$ is given by

$$\Delta(\theta_T)=[\phi(\omega_{\mathrm{SP}_N},\theta_1)-\phi(\omega_c,\theta_1)]^{1/2} \tag{4.4b}$$

for $\theta_T=\theta_1$, and ω_{SP} denotes $\omega_{\mathrm{SP}_N}^{+}$ and $\Delta(\theta_T)$ is given by

$$\Delta(\theta_T)=[\phi(\omega_{\mathrm{SP}_N}^{+},\theta_T)-\phi(\omega_c,\theta_T)]^{1/2} \tag{4.4c}$$

for $\theta_T>\theta_1$. The value of θ_s is defined as that value of θ_T at which the path of steepest descent through the neighboring saddle point crosses the pole, as described in Ref. 6. The proper phase of the multivalued function $\Delta(\theta_T)$ is then given by

$$arg[\Delta(\theta_T)]=\begin{cases}-\dfrac{\pi}{2}, & 1<\theta_T<\theta_s & (4.5a)\\ 0, & \theta_T=\theta_s & (4.5b)\\ \dfrac{3\pi}{4}, & \theta_T>\theta_s\,. & (4.5c)\end{cases}$$

Notice that $\theta_s>\theta_0$ for all values of ω_c in the domain $0<\omega_c\le(\omega_0^2-\delta^2)^{1/2}$, while $\theta_s=\theta_0$ for $\omega_c=0$. In Eq. (4.3), $F(\zeta)$ denotes Dawson's integral[26] and $\mathrm{erfc}(\zeta)$ denotes the complementary error function. The amplitude attenuation coefficient $\alpha(\omega_c)$ is given by

$$\alpha(\omega_c)=-\frac{1}{c}X(\omega_c)=\frac{\omega_c}{c}n_i(\omega_c)\,, \tag{4.6}$$

and where

$$k(\omega_c)=\frac{\omega_c}{c}n_r(\omega_c) \tag{4.7}$$

is the propagation factor at the real frequency ω_c in the dispersive medium.

Taken together, the expressions (4.3a), (4.3b), and (4.3d) constitute the uniform asymptotic approximation of the pole contribution at $\omega=\omega_c$ with $0<\omega_c\le(\omega_0^2-\delta^2)^{1/2}$; whereas the expressions (4.3a), (4.3c), and (4.3d) constitute the uniform asymptotic approximation of the pole contribution at $\omega=\omega_c=0$. For values of $\theta<\theta_s$ and sufficiently large observation distance z such that $|\Delta(\theta_T)|\sqrt{z/c}\gg 1$, the dominant term in the asymptotic expansion of the complementary error function may be substituted in Eq. (4.3a) with the result that the first and second terms in that equation identically cancel. Hence, for values of θ_T sufficiently less than θ_s there is no contribution to the asymptotic behavior of the total field from the simple pole singularity. For values of $\theta_T>\theta_s$ and sufficiently large observation distances z such that $|\Delta(\theta_T)|\sqrt{z/c}\gg 1$, the dominant term in the asymptotic expansion of $\mathrm{erfc}[-i\Delta(\theta_T)\sqrt{z/c}\,]$ may be substituted in Eq. (4.3d) with the result

$$U_c(z,t,T)\sim-e^{-z\alpha(\omega_c)}\sin[k(\omega_c)z-\omega_c t] \tag{4.8}$$

as $z\to\infty$ with θ_T bounded above θ_s.

The dynamical behavior of the pole contribution $U_c(z,t,T)$ as described by Eqs. (4.3a), (4.3b), and (4.3d) is illustrated in Fig. 10 as a function of the space-time parameter θ_T for a fixed carrier frequency $\omega_c=1\times10^{16}$/sec at the fixed propagation distance $z=1\times10^{-3}$ cm. For this particular case the steady-state amplitude attained by the field contribution $U_c(z,t,T)$ due to the simple pole singularity is an order of magnitude larger than that of

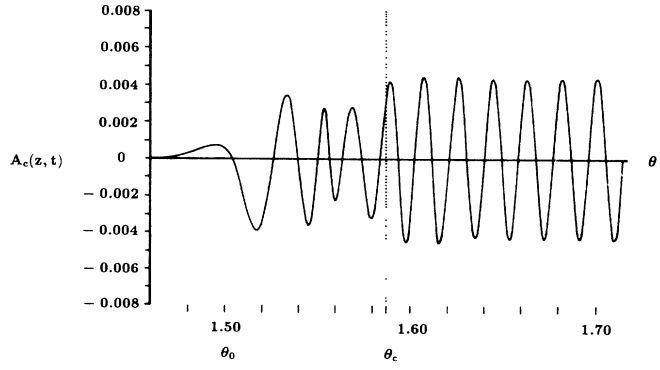

FIG. 10. Uniform asymptotic behavior of the pole contribution $U_c(z,t,T)$ for an input unit-step-function-modulated signal at $t=T$ with carrier frequency $\omega_c=1\times10^{16}$/sec at a propagation distance of $z=1\times10^{-3}$ cm in a highly absorptive and dispersive medium.

the peak in the Sommerfeld precursor field (see Fig. 6) and an order of magnitude less than that of the peak in the Brillouin precursor field (see Fig. 8). Notice that both the amplitude and the oscillation frequency of $U_c(z,t,T)$ settle down to their appropriate steady-state values, as described by Eq. (4.8), for $\theta_T > \theta_c > \theta_s$. Furthermore, for all $\theta_T > \theta_c$ the amplitude of the Brillouin precursor is less than that of $U_c(z,t,T)$ and is negligible for values of θ_T only slightly above θ_c. The value θ_c is associated with the signal arrival and is precisely defined in Sec. V.

B. Signal frequencies ω_c above the absorption band: $\omega_c \geq (\omega_1^2-\delta^2)^{1/2}$

For an input signal frequency ω_c in the domain $\omega_c \geq (\omega_1^2-\delta^2)^{1/2}$, which is above the medium absorption band, it is the distant saddle point in the right half of the complex ω plane that interacts with the simple pole singularity at $\omega=\omega_c$. The uniform asymptotic approximation of the pole contribution $U_c(z,t,T)$ is then given by the set of equations,[6]

$$U_c(z,t,T) \sim \frac{1}{2\pi}\mathrm{Re}\left[e^{i\omega_c T}\left\{-i\pi\,\mathrm{erfc}\left[-i\Delta(\theta_T)\left[\frac{z}{c}\right]^{1/2}\right]e^{(z/c)\phi(\omega_c,\theta_T)} - \frac{1}{\Delta(\theta_T)}\left[\frac{\pi c}{z}\right]^{1/2} e^{(z/c)\phi(\omega^+_{\mathrm{SP}_D},\theta_T)}\right\}\right], \quad 1 \leq \theta_T < \theta_s \tag{4.9a}$$

$$U_c(z,t,T) \sim \frac{1}{2\pi}\mathrm{Re}\left\{e^{i\omega_c T}\left[2\sqrt{\pi}e^{(z/c)\phi(\omega^+_{\mathrm{SP}_D},\theta_s)}F\left[|\Delta(\theta_s)|\left[\frac{z}{c}\right]^{1/2}\right] - \frac{1}{\Delta(\theta_s)}\left[\frac{\pi c}{z}\right]^{1/2} e^{(z/c)\phi(\omega^+_{\mathrm{SP}_D},\theta_s)}\right]\right\}$$
$$-\tfrac{1}{2}e^{-z\alpha(\omega_c)}\sin[k(\omega_c)z-\omega_c t_s'], \quad \theta_T=\theta_s=\frac{c}{z}t_s\ , \tag{4.9b}$$

$$U_c(z,t,T) \sim \frac{1}{2\pi}\mathrm{Re}\left[e^{i\omega_c T}\left\{i\pi\,\mathrm{erfc}\left[i\Delta(\theta_T)\left[\frac{z}{c}\right]^{1/2}\right]e^{(z/c)\phi(\omega_c,\theta_T)} - \frac{1}{\Delta(\theta_T)}\left[\frac{\pi c}{z}\right]^{1/2} e^{(z/c)\phi(\omega^+_{\mathrm{SP}_D},\theta_T)}\right\}\right]$$
$$-e^{-z\alpha(\omega_c)}\sin[k(\omega_c)z-\omega_c t], \quad \theta_T > \theta_s \tag{4.9c}$$

as $z \to \infty$, where $t_s' = t_s + T$ and where $F(\xi)$ again denotes Dawson's integral. The quantity $\Delta(\theta_T)$ is given by

$$\Delta(\theta_T) = [\phi(\omega^+_{\mathrm{SP}_D},\theta_T) - \phi(\omega_c,\theta_T)]^{1/2}\ , \tag{4.10}$$

with phase given by the relations

$$\frac{\pi}{4} \geq \arg[\Delta(\theta_T)] > 0, \quad 1 \leq \theta_T < \theta_s \tag{4.11a}$$

$$\arg[\Delta(\theta_s)] = 0, \quad \theta_T = \theta_s \tag{4.11b}$$

$$0 > \arg[\Delta(\theta_T)] \geq -\frac{3\pi}{4}, \quad \theta_T > \theta_s \tag{4.11c}$$

where $\arg[\Delta(\theta_T)]$ decreases monotonically with increasing θ_T.

Taken together, the expressions (4.9a)–(4.9c) constitute the uniform asymptotic approximation of the pole contribution at $\omega=\omega_c$ with finite $\omega_c \geq (\omega_1^2-\delta^2)^{1/2}$. For fixed values of $\theta_T < \theta_s$ and sufficiently large values of the propagation distance z such that the quantity $|\Delta(\theta_T)|\sqrt{z/c}$ is large ($\gg 1$), the dominant term in the asymptotic expansion of $\mathrm{erfc}[-i\Delta(\theta_T)\sqrt{z/c}\,]$ may be substituted into Eq. (4.9a) with the result that the first and second terms in that equation identically cancel. Hence, for values of θ sufficiently less than θ_s, there is no contribution to the asymptotic behavior of the total field from the simple pole singularity. On the other hand, for fixed values of $\theta > \theta_s$ and sufficiently large values of the observation distance z such that $|\Delta(\theta_T)|\sqrt{z/c} \gg 1$, the dominant term in the asymptotic expansion of $\mathrm{erfc}[i\Delta(\theta_T)\sqrt{z/c}\,]$ may be substituted into Eq. (4.9c) with the result

$$U_c(z,t,T) \sim -e^{-z\alpha(\omega_c)}\sin[k(\omega_c)z-\omega_c t] \tag{4.12}$$

as $z \to \infty$ with θ_T bounded above θ_s.

C. Signal frequencies ω_c in the absorption band: $(\omega_0^2-\delta^2)^{1/2} < \omega_c < (\omega_1^2-\delta^2)^{1/2}$

For values of the input signal frequency ω_c in the domain $(\omega_0^2-\delta^2)^{1/2} < \omega_c < (\omega_1^2-\delta^2)^{1/2}$, which is within the absorption band of the single-resonance Lorentz medium, neither the near nor distant saddle point comes within close proximity of the simple pole singularity at $\omega=\omega_c$. As a consequence, the quantity $|\Delta(\theta_T)|\sqrt{z/c}$ is large for all $\theta_T \geq 1$ and the dominant term in the corresponding asymptotic expansion of the complementary error function can be employed in the uniform asymptotic description of the pole contribution. For $\theta_T < \theta_s$ there is no contribution to the asymptotic behavior of the propagated field from the pole at $\omega=\omega_c$. At $\theta_T=\theta_s=ct_s/z$,

$$U_c(z,t_s',T) \sim -\tfrac{1}{2}e^{-z\alpha(\omega_c)}\sin[k(\omega_c)z-\omega_c t_s'] \tag{4.13}$$

as $z \to \infty$ with $t_s' = t_s + T$, and for $\theta_T > \theta_s$,

$$U_c(z,t,T) \sim -e^{-z\alpha(\omega_c)}\sin[k(\omega_c)z-\omega_c t] \tag{4.14}$$

as $z \to \infty$.

These equations are the same as the expressions that Brillouin[2,3] obtained for the pole contribution for all positive, finite values of the signal frequency ω_c. Even the value of the space-time parameter θ_T at which the discontinuous jump in the behavior of $U_c(z,t,T)$ occurs

in Eqs. (4.3), (4.9), and (4.13)–(4.14) is the same as that obtained by Brillouin because θ_s is taken in the uniform asymptotic expansion presented here to be the value of θ_T at which the path of steepest descent crosses the simple pole singularity at $\omega=\omega_c$. The nonuniform asymptotic analysis presented by Oughstun and Sherman[5] yields the same expressions for $U_c(z,t,T)$ as obtained by Brillouin, but the value of θ_s can be different since θ_s is then the value of θ_T at which an arbitrary Olver-type path[25] crosses the pole. The difference in values obtained for θ_s is of no consequence, however, since $U_c(z,t,T)$ is asymptotically negligible in the final expression for the total propagated field $U(z,t,T)$ for values of θ_T in a range that includes all possible values of θ_s.[6] Although Brillouin associated $\theta_s=ct_s/z$ with the time of arrival of the main signal, that interpretation has been shown to be incorrect.[4–6,12]

V. THE SIGNAL ARRIVAL AND THE SIGNAL VELOCITY

The contribution of the simple pole singularity at $\omega=\omega_c$ to the uniform asymptotic description of $U(z,t,T)$ occurs when the original contour of integration C, which extends along the straight line from $ia-\infty$ to $ia+\infty$ in the upper half of the complex ω plane, lies on the opposite side of the pole singularity than does the Olver-type path $P(\theta_T)$ through the relevant saddle points.[6] For $\theta_T<\theta_s$ the pole is not crossed when C is deformed to $P(\theta_T)$ and there is no residue contribution, while for $\theta_T>\theta_s$ the pole is crossed when C is deformed to $P(\theta_T)$ and there is a residue contribution to the asymptotic behavior of the field. The value of θ_s clearly depends upon which Olver-type path is chosen for $P(\theta_T)$. If that path is taken to lie along the path of steepest descent through the saddle point nearest the pole, then the value of θ_s is specified by the expression

$$Y(\omega_{\rm SP},\theta_s)=Y(\omega_c,\theta_s)\ , \tag{5.1}$$

where $\omega_{\rm SP}(\theta_T)$ denotes the saddle point which interacts with the simple pole singularity. However, at $\theta_T=\theta_s$ the pole contribution is asymptotically negligible in comparison to the saddle point contribution since $P(\theta_T)$ is an Olver-type path. Consequently, the particular value of θ_s at which the pole crossing occurs has no physical importance in the asymptotic behavior of the propagated field, in spite of the fact that it is an important parameter in the uniform asymptotic description of the pole contribution to the propagated field $U(z,t,T)$.

The pole contribution at $\omega=\omega_c$ is the dominant contribution to the asymptotic behavior of the propagated field $U(z,t,T)$ for $\theta_T>\theta_c>\theta_s$, where θ_c is specified by the relation

$$X(\omega_{\rm SP},\theta_c)=X(\omega_c)\ , \tag{5.2}$$

where $\omega_{\rm SP}$ denotes the dominant saddle point at the value of θ_T, and where $X(\omega,\theta_T)={\rm Re}[\phi(\omega,\theta_T)]$ is independent of θ_T along the real frequency axis. For values of $\theta_T<\theta_c$ such that the inequality $X(\omega_{\rm SP},\theta_T)>X(\omega_c)$ is satisfied, the saddle point is the dominant contribution to the asymptotic behavior of the field $U(z,t,T)$ and the pole contribution is asymptotically negligible by comparison. For values of $\theta_T>\theta_c$ such that the inequality $X(\omega_{\rm SP},\theta_T)<X(\omega_c)$ is satisfied, the pole contribution is the dominant contribution to the asymptotic behavior of $U(z,t,T)$ and the saddle point contribution is asymptotically negligible by comparison. From Eqs. (4.8), (4.12), and (4.14) this pole contribution, when it is the dominant contribution to the asymptotic behavior of the field $U(z,t,T)$, is given by

$$U_c(z,t,T)\sim -e^{-z\alpha(\omega_c)}\sin[k(\omega_c)z-\omega_c t]\ , \tag{5.3}$$

as $z\to\infty$ with $\theta_T>\theta_c$.

The pole contribution (5.3) is physically due to the frequency component at the applied frequency ω_c of the input unit-step-function-modulated signal. The main signal arrival is defined to occur at the value of $\theta_T=\theta_c$ specified by the relation[5]

$$X(\omega^{+}_{{\rm SP}_N},\theta_c)=X(\omega_c),\quad \theta_c\geq\theta_0 \tag{5.4}$$

at which the pole contribution becomes the dominant contribution to the asymptotic behavior of the field $U(z,t,T)$. The velocity at which this point in the field propagates through the dispersive medium is defined as the main signal velocity

$$v_c=\frac{c}{\theta_c}\ , \tag{5.5}$$

where c is the vacuum speed of light. Furthermore, for signal frequencies $\omega_c>\omega_{SB}$ a prepulse exists in the evolution of the field due to the input unit-step-function-modulated signal.[5,6] The front of the prepulse arrives at the value of $\theta_T=\theta_{c1}$ specified by the relation

$$X(\omega^{+}_{{\rm SP}_D},\theta_{c1})=X(\omega_c),\quad 1<\theta_{c1}<\theta_{SB}\ , \tag{5.6}$$

and the velocity at which this point propagates through the dispersive medium, called the anterior presignal velocity, is given by

$$v_{c1}=\frac{c}{\theta_{c1}},\quad \omega_c>\omega_{SB}\ . \tag{5.7}$$

The back of the prepulse arrives at the value of $\theta_T=\theta_{c2}$ specified by the relation

$$X(\omega_{{\rm SP}_1},\theta_{c2})=X(\omega_c),\quad \theta_{SB}<\theta_{c2}<\theta_0\ , \tag{5.8}$$

and the velocity at which this point propagates through the dispersive medium, called the posterior presignal velocity, is given by

$$v_{c2}=\frac{c}{\theta_{c2}},\quad \omega_c>\omega_{SB}\ . \tag{5.9}$$

These three velocities are then seen to satisfy the inequality

$$c>v_{c1}>\frac{c}{\theta_{SB}}>v_{c2}>\frac{c}{\theta_0}\geq v_c\ , \tag{5.10}$$

as illustrated in Fig. 11(a). The dashed curve in the figure

depicts the energy transport velocity of a strictly monochromatic field in the dispersive medium, as described by Loudon.[13]

The transition points θ_c, θ_{c1}, and θ_{c2} in the dynamical field evolution of the unit-step-function-modulated signal in the mature dispersion regime are physically characterized by the instantaneous angular frequency of oscillation of the total field evolution at any fixed propagation distance z, dependent upon whether $0 \leq \omega_c < \omega_{SB}$ or $\omega_c > \omega_{SB}$. Consider first the behavior for $\omega_c \in [0, \omega_{SB})$, in which case only the transition point θ_c occurs. For $\theta_T < \theta_c$ the field $U(z,t,T)$ is either dominated by the

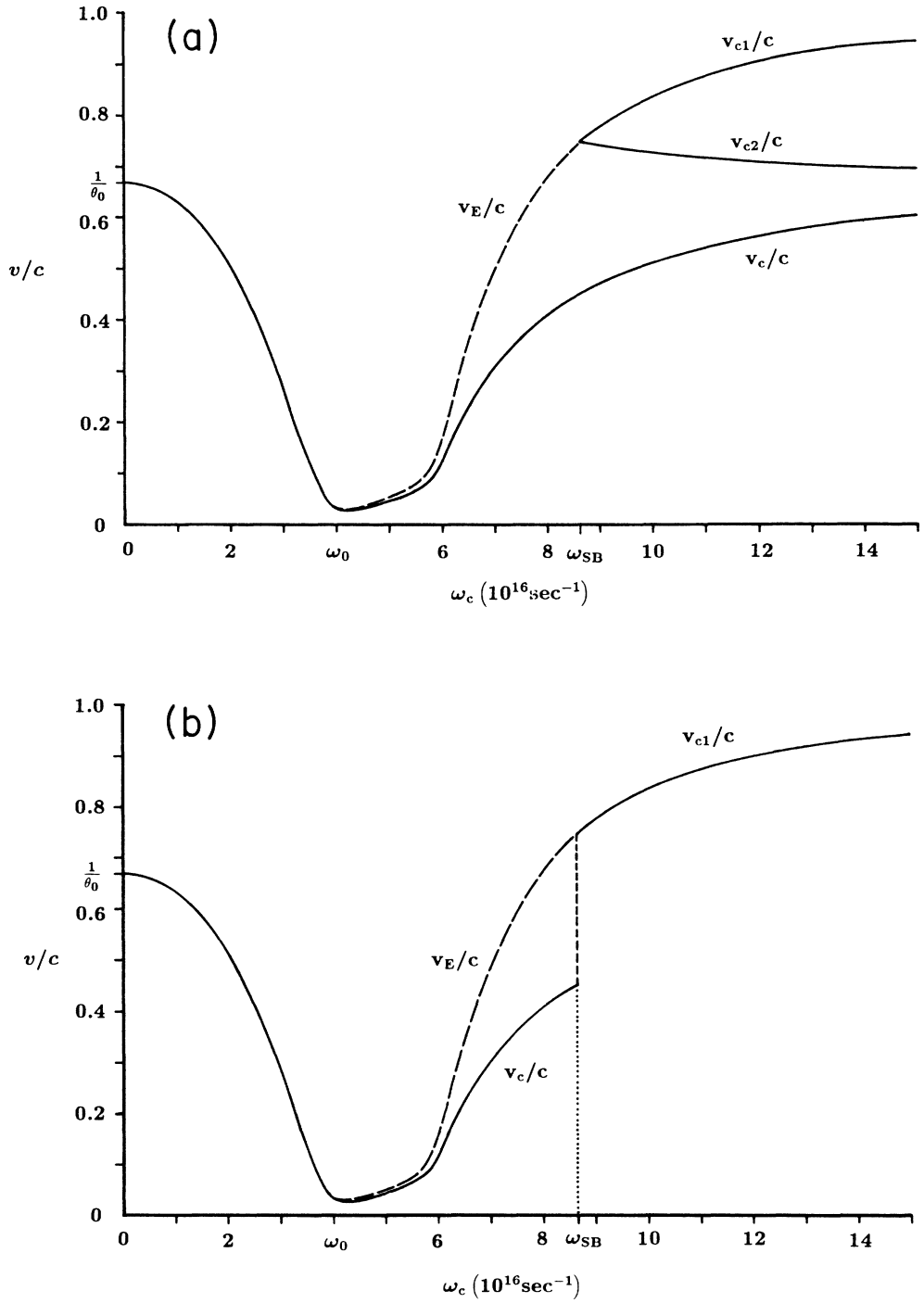

FIG. 11. Frequency dependence of (a) the main signal, anterior presignal, and posterior presignal velocities for a unit-step-function signal, and (b) the signal velocity for a rectangular pulse in a Lorentz medium with $\omega_0 = 4 \times 10^{16}/\text{sec}$, $b^2 = 20 \times 10^{32}/\text{sec}^2$, $\delta = 0.28 \times 10^{16}/\text{sec}$. The behavior of the energy-transport velocity for a strictly monochromatic field in the medium is indicated by the dashed curve in both figures.

Sommerfeld precursor whose instantaneous angular frequency $\omega_s \simeq \xi(\theta_R) = \mathrm{Re}[\omega^+_{SP_D}(\theta_T)]$ rapidly decreases from infinity at $\theta_T = 1$ and monotonically approaches the limiting value $(\omega_1^2 - \delta^2)^{1/2}$ from above as $\theta_T \to \infty$ but only reaches the value ω_{SB} at $\theta_T = \theta_{SB}$ (because of the transition to the Brillouin precursor), or is dominated by the Brillouin precursor whose instantaneous angular frequency $\omega_B \simeq \psi(\theta_T) = \mathrm{Re}[\omega^+_{SP_N}(\theta_T)]$ is either approaching ω_c from below if $\omega_c \leq (\omega_0^2 - \delta^2)^{1/2}$, or is bounded below ω_c for all θ_T if $(\omega_1^2 - \delta^2)^{1/2} < \omega_c < \omega_{SB}$. Only for $\theta_T > \theta_c$ does the field oscillate predominantly at the input carrier frequency ω_c of the signal. When $\omega_c > \omega_{SB}$ the dynamical field evolution is greatly enriched because of the additional two transition points θ_{c1} and θ_{c2}. For $\theta_T < \theta_{c1}$ the field is dominated by the Sommerfeld precursor whose instantaneous oscillation frequency ω_s approaches ω_c from above as θ_T approaches θ_{c1} from below. For all θ_T in the space-time interval $\theta_{c1} < \theta_T < \theta_{c2}$, the field oscillates predominantly at the input carrier frequency ω_c of the signal. This portion of the signal evolution is interrupted by the Brillouin precursor which dominates the field evolution over the space-time interval $\theta_{c1} < \theta_T < \theta_c$ and is characterized by an instantaneous oscillation frequency that is bounded below ω_c. Again, for $\theta_T > \theta_c$ the field oscillates predominantly at ω_c. This description afforded by the asymptotic theory has been completely verified through numerical simulations.[12] Finally, the branching character of the signal velocity for $\omega_c > \omega_{SB}$ is a direct consequence of the asymptotic dominance of the second precursor field for $\theta_{c2} < \theta_T < \theta_c$.

For an input rectangular modulated signal $A(z,t) = U(z,t,0) - U(z,t,T)$ of initial time duration T and carrier frequency $\omega_c \in [0, \omega_{SB})$, the signal arrival occurs at $\theta = \theta_c$ and the propagated field ceases to oscillate at ω_c when $\theta_T = \theta - cT/z = \theta_c$. Both of these transition points propagate with the signal velocity $v_c = c/\theta_c$. The main body of the propagated pulse that is oscillating at $\omega = \omega_c$ then evolves over the space-time interval from $\theta = \theta_c$ to $\theta = \theta_c + cT/z$. The θ width of the propagated pulse between the front and back pole contributions is then $\Delta\theta_c = cT/z$ so that the corresponding temporal width of the pulse between these two points at any fixed propagation distance z is

$$\Delta t_c = \frac{z}{c}\Delta\theta_c = T \ . \tag{5.11}$$

Consequently, any pulse broadening and envelope degradation of the input rectangular modulated pulse with $\omega_c \in [0, \omega_{SB})$ is due primarily to the precursor field structure of the propagated field that arises from the front and back of the input field. This interference of the pole contribution with the precursor field structure will shorten the θ domain over which the propagated field oscillates predominantly at the input carrier frequency ω_c. Strictly speaking, the temporal width of the signal is then found to decrease with increasing propagation distance. The commonly observed phenomenon[15–20] of pulse spreading is obtained only when the propagated signal is redefined so as to include a range of frequencies about ω_c, and this in turn implies the incorporation of some portion of the precursor fields in the definition of the main body of the pulse.

For $\omega_c > \omega_{SB}$ the signal arrival first occurs at $\theta = \theta_{c1}$ when the simple pole at $\omega = \omega_c$ is crossed and the propagated field finally ceases to oscillate predominantly at ω_c when $\theta_T = \theta - cT/z = \theta_{c1}$ when the pole contribution is subtracted out. The overall θ width of the propagated pulse between the front and back contributions is then $\Delta\theta_c = cT/z$ so that the corresponding temporal width of the pulse between these two points at any fixed propagation distance z is

$$\Delta t_c = \frac{z}{c}\Delta\theta_c = T \ . \tag{5.12}$$

Between these two space-time points there are, at most, two other distinct transition points at $\theta = \theta_{c2}$ and θ_c at which the propagated field either ceases to oscillate predominantly at ω_c or begins again to oscillate predominantly at $\omega = \omega_c$ due to the asymptotic dominance of the leading edge Brillouin precursor between these two points. Because of this, the propagated field due to the input rectangular pulse separates into, at most, two subpulses (provided that $cT/z > \theta_c - \theta_{c1}$), which reduce to a single pulse at sufficiently large propagation distances. Apart from this pulse breakup, the only other envelope degradation and any pulse broadening of the input rectangular modulated pulse with $\omega_c > \omega_{SB}$ is due to the precursor field structure of the propagated field that arises from the front and back of the input field.

The resultant frequency dependence of the signal velocity for a finite duration rectangular pulse with $cT/z < \theta_c - \theta_{c1}$ is illustrated in Fig. 11(b). As in Fig. 11(a), the dashed curve represents the energy transport velocity of a strictly monochromatic field in the medium. The discontinuous jump in the signal velocity at $\omega_c = \omega_{SB}$ is fundamentally due to the change in dominance of the precursor fields at $\theta = \theta_{SB}$. Below ω_{SB} the signal arrival occurs following the evolution of the Sommerfeld and Brillouin precursors, while above ω_{SB} the signal arrival occurs during the evolution of the Sommerfeld precursor field. When the opposite inequality is satisfied (i.e., when $cT/z > \theta_c - \theta_{c1}$) by choosing a sufficiently long initial pulse width T or a sufficiently short propagation distance z (but which is still large enough to be in the mature dispersion regime), then the propagated field is found to be separated into two pulses whose velocities are described in Fig. 11(a). The first is a prepulse with front velocity v_{c1} and back velocity v_{c2}, and the second subpulse has front velocity v_c and back velocity v_{c1}.

VI. DYNAMICAL EVOLUTION OF THE PROPAGATED FIELD

From Eq. (1.34), the uniform asymptotic description of the propagated field due to an input rectangular-modulated signal of initial time duration T is given by the representation

$$A(z,t) \sim U_S(z,t,0) + U_B(z,t,0) + U_c(z,t,0) - U_S(z,t,T) - U_B(z,t,T) - U_c(z,t,T) \ , \tag{6.1}$$

which is simply the difference between the propagated fields due to an input unit-step-function-modulated signal $U(z,t,0) \sim U_S(z,t,0) + U_B(z,t,0) + U_c(z,t,0)$ that begins to oscillate at time $t=0$ in the $z=0$ plane and the unit step-function-modulated signal $U(z,t,T) \sim U_S(z,t,T) + U_B(z,t,T) + U_c(z,t,T)$ that begins to oscillate at time $t=T$ in the $z=0$ plane. It is now shown that this representation of the propagated field in the mature dispersion limit provides a complete, accurate representation of the dynamical field evolution over the entire range of signal frequencies $\omega_c \in [0, \infty)$.

Consider first the below resonance range $\omega_c \in [0, \omega_0)$. In this case the peak Sommerfeld precursor field amplitude is typically several orders of magnitude less than the peak amplitude of the Brillouin precursor so that the entire propagated field structure in the mature dispersion limit is dominated by the Brillouin precursor and the pole contribution at $\omega = \omega_c$. For a sufficiently long initial pulse width T and/or a sufficiently short propagation distance z such that $(c/z)T > \theta_c - 1$, the precursor fields associated with the leading edge $U(z,t,0)$ of the pulse will completely evolve prior to the arrival of the precursor fields associated with the trailing edge $U(z,t,T)$ of the pulse. Indeed, the trailing edge precursors will arrive only after the main signal of the leading edge has arrived (at $\theta = \theta_c$) and is evolving. Hence, when this condition prevails the interference between the precursor fields of the leading and trailing edges of the pulse is minimal and the pulse distortion is also minimal, as is evident in Fig. 12. For shorter initial pulse widths T or larger propagation distances z such that $\theta_c - 1 > (c/z)T > \theta_{SB} - 1$, the first precursor field associated with the leading edge of the pulse will still evolve undisturbed, but during the evolution of the second precursor field $U_B(z,t,0)$ the arrival and evolution of the precursor fields associated with the trailing edge of the pulse will occur. Hence, when this condition prevails there will be interference between the Brillouin precursor of the leading edge and the Sommerfeld precursor of the trailing edge of the pulse, as illustrated in Fig. 13, and the Brillouin precursor of the trailing edge of the pulse will occur soon after the signal arrival at $\theta = \theta_c$ so that the resultant pulse distortion is found to be moderate. Finally, for even shorter initial pulse widths T or greater propagation distances z such that $0 < (c/z)T \leq \theta_{SB} - 1$, there will be a nearly complete overlap of these two sets of precursors fields and the resultant pulse distortion is severe, as illustrated in Fig. 14.

In each case the pole contribution to the total field evolution occurs at $\theta = \theta_c$ and is subtracted out at $\theta = \theta_c + cT/z$ so that the overall temporal width of the propagated signal is T, as given by Eq. (5.11). However, because of the asymptotic dominance of the Brillouin precursor $U_B(z,t,T)$ from the back edge of the input

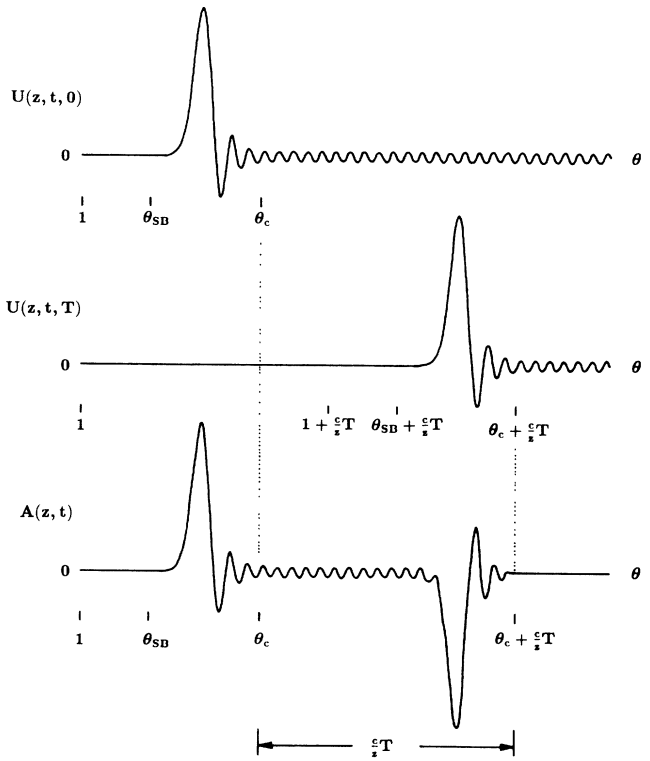

FIG. 12. Construction of the dynamical structure of the propagated field $A(z,t) = U(z,t,0) - U(z,t,T)$ in the below resonance signal frequency range $0 < \omega_c < \omega_0$ when $(c/z)T > \theta_c - 1$. When this situation prevails the interference between the precursor fields of the leading and trailing edges of the pulse is minimal and the resultant pulse distortion is also minimal.

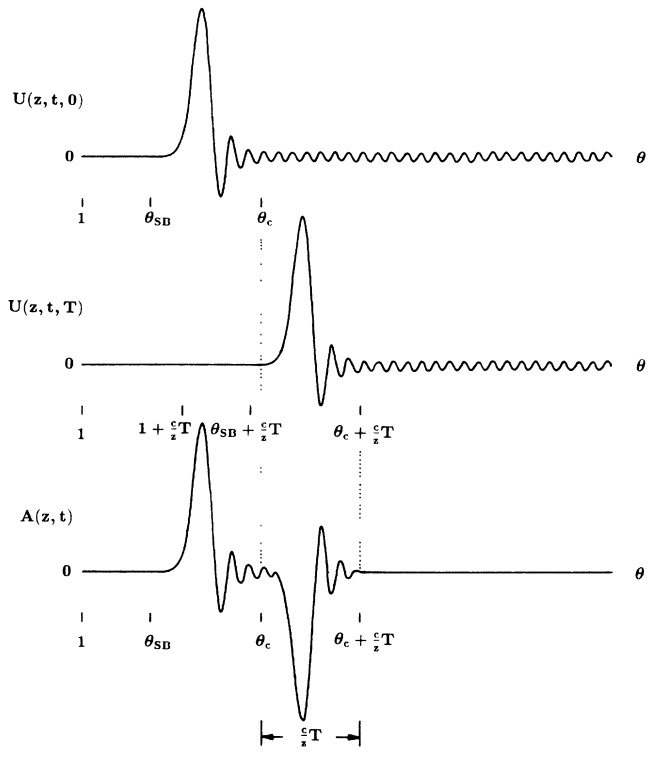

FIG. 13. Construction of the dynamical structure of the propagated field $A(z,t) = U(z,t,0) - U(z,t,T)$ in the below resonance signal frequency range $0 < \omega_c < \omega_0$ when $\theta_c - 1 > (c/z)T > \theta_{SB} - 1$. When this situation prevails the interference between the precursor fields of the leading and trailing edges of the pulse is moderate and the resultant pulse distortion is also moderate.

pulse, the propagated signal is the dominant contribution to the total field evolution only over the θ domain from $\theta=\theta_c$ to $\theta\cong\theta_0+cT/z$. The corresponding temporal width of the propagated signal is then

$$\Delta t_s \cong T-\frac{z}{c}(\theta_c-\theta_0)\ , \tag{6.2}$$

provided that $\theta_0+cT/z>\theta_c$, which is satisfied up through most of the moderate distortion range. When the opposite inequality (i.e., $\theta_0+ct/z\le\theta_c$) is satisfied, the pulse distortion is severe and the total propagated field is dominated by the precursor fields over the entire space-time domain.

Similar results hold in the signal frequency domain $\omega_c\in[\omega_0,\omega_{SB}]$, which contains the medium absorption band $[\omega_0,\omega_1]$ and proceeds up to the signal frequency ω_{SB} at which the signal velocity of the unit-step-function-modulated signal bifurcates. The only difference from the preceding case is that the Sommerfeld precursor field structure now becomes more pronounced in the total field evolution as the spectral amplitude of each unit-step-function-modulated signal increases in the above resonance frequency domain. The construction of the propagated field structure in the severe distortion limit $0<(c/z)T\le\theta_{SB}-1$ is illustrated in Fig. 15 for a signal frequency ω_c that is near resonance. For initial pulse widths T and propagation distances z satisfying this inequality there is a nearly complete overlap of the two sets of precursor fields so that the propagated field structure $A(z,t)$ is dominated by a pair of interfering Sommerfeld precursors followed by a pair of interfering Brillouin precursors, which is then followed by the signal oscillating at $\omega=\omega_c$ that evolves over the space-time interval from $\theta=\theta_c$ to θ_c+cT/z, as illustrated. Just prior to the signal arrival at $\theta=\theta_c$ the field is dominated by the interfering pair of Brillouin precursor fields whose instantaneous oscillation frequency is less than ω_c.

In the low-frequency region of the signal frequency domain $[\omega_0,\omega_{SB}]$ the Sommerfeld precursor field is relatively insignificant in comparison to both the Brillouin precursor field and the pole contribution so that Eq. (6.2) applies for the temporal width of the propagated signal. On the other hand, in the high-frequency region of this signal frequency domain the Sommerfeld precursor is a dominant feature in the total propagated field over the space-time domains $\theta\in[1,\theta_{SB})$ and $\theta_T\in[1,\theta_{SB})$. The propagated signal, which arises from the pole contribution that evolves over the space-time domain from $\theta=\theta_c$ to θ_c+cT/z, is then seen to be the dominant contribution to the total field over the θ domain from $\theta=\theta_c$ to $1+cT/z$ when $cT/z>\theta_c-1$, with temporal width

$$\Delta t_s=T-\frac{z}{c}(\theta_c-1)\ , \tag{6.3}$$

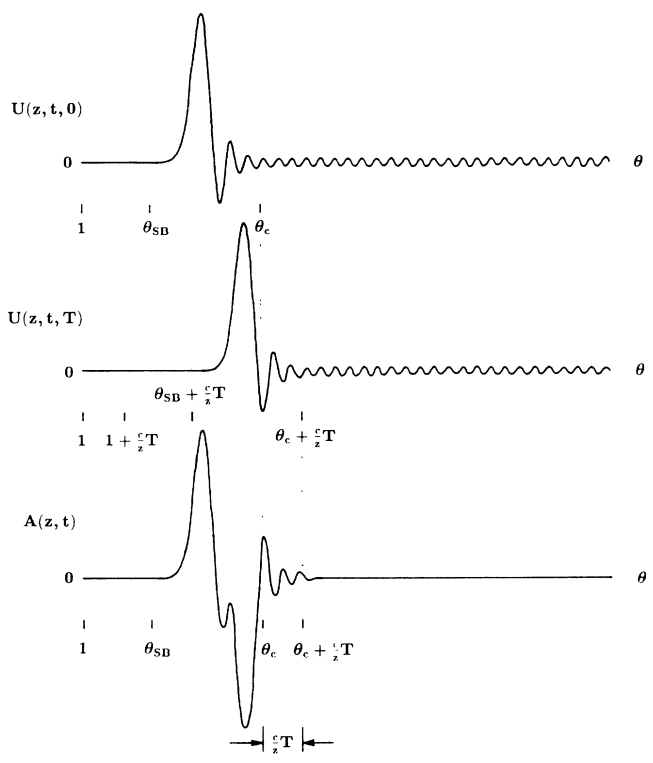

FIG. 14. Construction of the dynamical structure of the propagated field $A(z,t)=U(z,t,0)-U(z,t,T)$ in the below resonance signal frequency range $0<\omega_c<\omega_0$ when $(c/z)T\le\theta_{SB}-1$. When this situation prevails the interference between the precursor fields of the leading and trailing edges of the pulse is nearly complete and the resultant pulse distortion is severe.

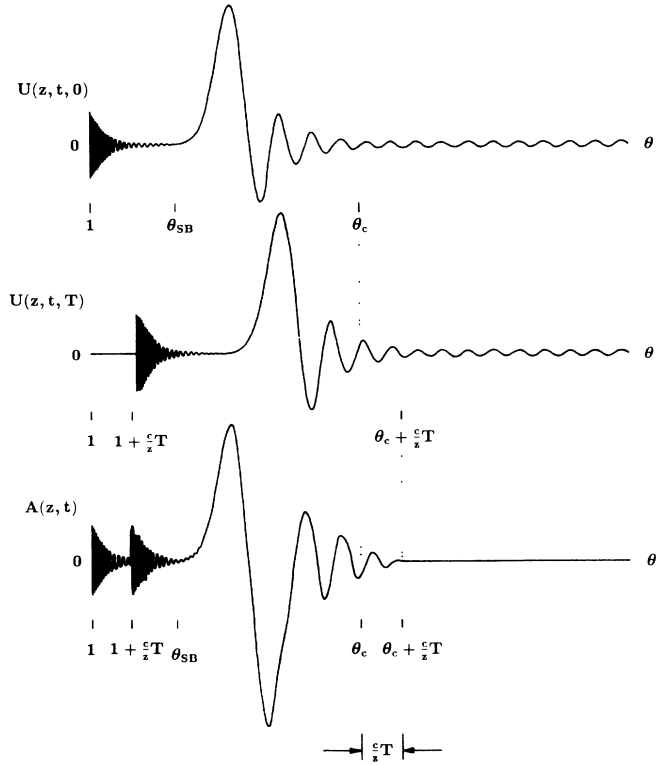

FIG. 15. Construction of the dynamical structure of the propagated field $A(z,t)=U(z,t,0)-U(z,t,T)$ for a near resonance signal frequency $\omega_c\in[\omega_0,\omega_1]$ when $(c/z)T\le\theta_{SB}-1$. When this situation prevails the interference between the precursor fields of the leading and trailing edges of the pulse is nearly complete and the resultant pulse distortion is severe.

and is then again the dominant contribution over a small θ interval about the space-time point $\theta=\theta_{SB}+cT/z$ provided that $cT/z \gtrsim \theta_c-\theta_{SB}$. When the first inequality (i.e., $cT/z>\theta_c-1$) is satisfied, the propagated signal is seen to be separated into two pulses oscillating at $\omega=\omega_c$. These reduce to a single pulse oscillating at $\omega=\omega_c$ when $\theta_c-1 \geq cT/z \gtrsim \theta_c-\theta_{SB}$. Finally, when the inequality $cT/z \lesssim \theta_c-\theta_{SB}$ is satisfied, the pulse distortion is severe and the total propagated field is dominated by the precursor fields over the entire space-time domain.

Consider, finally, the high-frequency domain $\omega_c>\omega_{SB}$ in which the propagated unit-step-function-modulated signal separates into a prepulse that evolves over the space-time domain $\theta\in[\theta_{c1},\theta_{c2}]$ and a main signal that evolves over the space-time domain $\theta>\theta_c$, these two signal components being separated by the Brillouin precursor field which is the asymptotically dominant field contribution over the domain $\theta\in(\theta_{c2},\theta_c)$, as described in Refs. 4–6. In this high-frequency domain the Sommerfeld precursor field is a dominant feature in the total field evolution of the propagated unit-step-function-modulated signal and is the asymptotically dominant field contribution over the space-time domain $\theta\in[1,\theta_{c1})$. For a sufficiently long initial pulse width T and/or a sufficiently small propagation distance z such that $(c/z)T>\theta_c-1$, the precursor fields and prepulse associated with the leading edge $U(z,t,0)$ of the pulse will completely evolve prior to the arrival and evolution of the precursors and prepulse associated with the trailing edge $U(z,t,T)$ of the pulse so that their interference is minimal. When this condition prevails the total propagated field evolves in the following sequential manner [the leading term in each asymptotic expression given here and in the following expressions of this section indicates that it is asymptotically dominant over the remaining terms (if any)]:

$1\leq\theta<\theta_{c1}$	$A(z,t)\sim U_S(z,t,0)$	Sommerfeld precursor
$\theta_{c1}\leq\theta\leq\theta_{c2}$	$A(z,t)\sim U_c(z,t,0)$	Signal
$\theta_{c2}<\theta<\theta_c$	$A(z,t)\sim U_B(z,t,0)+U_c(z,t,0)$	Brillouin precursor plus signal
$\theta_c\leq\theta<1+\frac{c}{z}T$	$A(z,t)\sim U_c(z,t,0)$	Signal
$1+\frac{c}{z}T\leq\theta<\frac{c}{z}T+\theta_{c1}$	$A(z,t)\sim -U_S(z,t,T)+U_c(z,t,0)$	Sommerfeld precursor plus signal
$\theta_{c1}+\frac{c}{z}T\leq\theta<\theta_{SB}+\frac{c}{z}T$	$A(z,t)\sim -U_S(z,t,T)$	Sommerfeld precursor
$\theta_{SB}+\frac{c}{z}T<\theta$	$A(z,t)\sim -U_B(z,t,T)$	Brillouin precursor

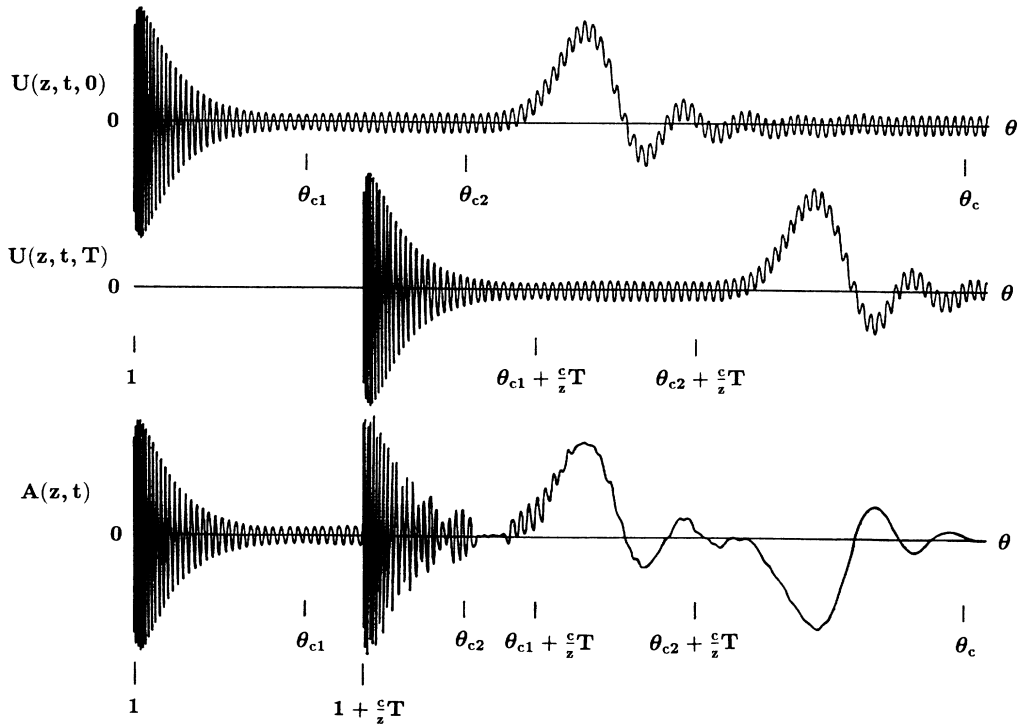

FIG. 16. Construction of the dynamical structure of the propagated field $A(z,t)-U(z,t,0)-U(z,t,T)$ in the high signal frequency range $\omega_c>\omega_{SB}>\omega_0$ when $\theta_{c1}-1<(c/z)T<\theta_{c2}-1$. When this situation prevails the interference between the precursor fields of the leading and trailing edges of the pulse is moderate to severe and the resultant pulse distortion is becoming severe.

The propagated signal is thus separated into a prepulse that evolves over the space-time domain $\theta\in[\theta_{c1},\theta_{c2}]$ with temporal width

$$\Delta t_p=\frac{z}{c}(\theta_{c2}-\theta_{c1}) , \tag{6.4}$$

which increases linearly with the propagation distance, and a main pulse that evolves over the space-time domain $\theta\in[\theta_c,1+(c/z)T]$ with temporal width

$$\Delta t_s=T-\frac{z}{c}(\theta_c-1) , \tag{6.5}$$

which decreases to zero linearly with the propagation distance z over the propagation domain $(c/z)T>\theta_c-1$. The front and back of the prepulse then propagate with the presignal velocities $v_{c1}=c/\theta_{c1}$ and $v_{c2}=c/\theta_{c2}$, respectively, while the front of the main pulse propagates with the signal velocity $v_c=c/\theta_c$, just as for the unit-step-function-modulated signal. A moments reflection on the limiting behavior of this pulse structure as the propagation distance z becomes small (ignoring momentarily that the above results are derived from asymptotic theory) shows that the prepulse width (6.4) approaches zero while the main pulse width (6.5) approaches the initial pulse width T. The main pulse is then clearly associated with the initial rectangular pulse. As the propagation distance z increases so that the inequality $(c/z)T<\theta_c-1$ is satisfied, the main pulse vanishes from the propagated field structure and all that remains is the prepulse and the precursor fields. The prepulse remains intact, evolving undisturbed over the space-time domain $[\theta_{c1},\theta_{c2}]$ until the inequality $(c/z)T<\theta_{c2}-1$ is satisfied. When this latter condition prevails the prepulse becomes distorted as the Sommerfeld precursor associated with the back edge of the pulse evolves over this space-time domain. This situation is illustrated in Fig. 16 when $\theta_{c1}-1<(c/z)T<\theta_{c2}-1$. When this condition prevails the total propagated field evolves in the following sequential manner:

$1\le\theta<\theta_{c1}$	$A(z,t)\sim U_S(z,t,0)$	Sommerfeld precursor
$\theta_{c1}\le\theta<1+\frac{c}{z}T$	$A(z,t)\sim U_c(z,t,0)$	Signal
$1+\frac{c}{z}T\le\theta\le\theta_{c2}$	$A(z,t)\sim -U_S(z,t,T)+U_c(z,t,0)$	Sommerfeld precursor plus signal
$\theta_{c2}<\theta<\theta_{c1}+\frac{c}{z}T$	$A(z,t)\sim A_B(z,t,0)-U_S(z,t,T)+U_c(z,t,0)$	Brillouin and Sommerfeld precursors plus signal
$\theta_{c1}+\frac{c}{z}T<\theta<\theta_{c2}+\frac{c}{z}T$	$A(z,t)\sim A_B(z,t,0)$	Brillouin precursor
$\theta_{c2}+\frac{c}{z}T<\theta$	$A(z,t)\sim -A_B(z,t,T)+A_B(z,t,0)$	Brillouin precursors

The propagated field structure is then seen to be dominated by the precursor fields associated with the front and back of the pulse over all but the domain $\theta\in[\theta_{c1},1+(c/z)T]$. The temporal width of the prepulse is now given by

$$\Delta t_p=T-\frac{z}{c}(\theta_{c1}-1) , \tag{6.6}$$

which decreases from its maximum value of $(z/c)(\theta_{c2}-\theta_{c1})$ when $(c/z)T=\theta_{c2}-1$ and goes to zero when $(c/z)T=\theta_{c1}-1$ as the propagation distance z increases.

The validity of this uniform asymptotic description of rectangular pulse propagation in a single-resonance Lorentz medium is borne out by comparison with detailed numerical calculations of the dynamical pulse evolution. The calculations presented here are for a strongly absorptive medium with parameters $\omega_0=4.0\times10^{16}$/sec, $b^2=20.0\times10^{32}$/sec, $\delta=0.28\times10^{16}$/sec, which are the same as those chosen by Brillouin.[2,3] The dynamical evolution of the propagated field at several increasing values of the propagation distance z is illustrated in Figs. 17–20 for the below resonance signal frequency $\omega_c=1.0\times10^{16}$/sec. The e^{-1} penetration depth at this signal frequency is $d=1.82\times10^{-4}$ cm. In each sequence of propagated waveforms the time origin has been shifted by the amount $\theta_c z/c$ so that the signal arrival at $\theta_c z/c$ and signal departure at $t=\theta_c z/c+T$ are aligned at each propagation distance; these time instances are indicated by the dotted lines in each figure. The initial pulse width in Fig. 17 is $T=6.283\times10^{-16}$ sec and corresponds to a single period of oscillation of the signal. In this case the pulse distortion becomes severe $(cT/z<\theta_{SB}-1)$ after only $\sim\frac{1}{3}$ of an absorption depth into the medium, after which the propagated waveform is dominated by the interfering Brillouin precursors from the leading and trailing edges of the pulse. In Fig. 18 the initial pulse width is doubled to $T=1.257\times10^{-15}$ sec and corresponds to two periods of oscillation of the input signal. In this case the pulse distortion is minimal when $z/d=0.055$, moderate when $z/d=0.55$, and severe when $z/d=2.75$ and all larger propagation distances. Each of these cases corresponds qualitatively to the constructions depicted in Figs. 12–14, respectively. The initial pulse width is again doubled to $T=2.513\times10^{-15}$ sec in Fig. 19. In this case the pulse distortion is minimal when $z/d\le0.7d$ and becomes severe when $z/d=1.24d$, after which the propagated waveform is dominated by the interfering Brillouin precursors. Finally, the initial pulse width is doubled once more to $t=5.026\times10^{-15}$ sec in Fig. 20, which corre-

sponds to eight periods of oscillation of the input signal. In this case the transition from minimal to moderate pulse distortion occurs when $z=1.41d$ and the transition to severe pulse distortion occurs when $z=2.48d$. By comparison, the transition to the severe pulse distortion regime for a picosecond pulse occurs when $z\sim 500d$. Again, in the severe pulse distortion regime the propagated waveform is dominated by the interfering Brillouin precursors. Similar results have been obtained numerically by Barakat[27] for a Lorentz medium and by Albanese, Penn, and Medina[28] for a Debye model medium.

Careful inspection of Figs. 17–20 shows that the propagated pulse-signal width given by Eq. (6.2) correctly describes the time duration over which the propagated waveform is dominated by the signal oscillating at the input signal frequency ω_c. In particular, this pulse-signal width is seen to decrease with increasing propagation distance z from its input value T to zero at the transition point to the severe distortion limit. Nevertheless, the overall temporal width of the entire propagated waveform is seen to increase with the propagation distance z. Up into the severe distortion regime the propagated pulse waveform is seen to be defined between $\theta=\theta_0$ and θ_c+cT/z, with corresponding temporal width

$$\Delta t = T+\frac{z}{c}(\theta_c-\theta_0)\ . \tag{6.7}$$

Once into the severe distortion regime, the propagated field structure becomes completely dominated by the front and back Brillouin precursors whose peak values occur at $\theta=\theta_0$ and θ_0+cT/z and are thus separated in

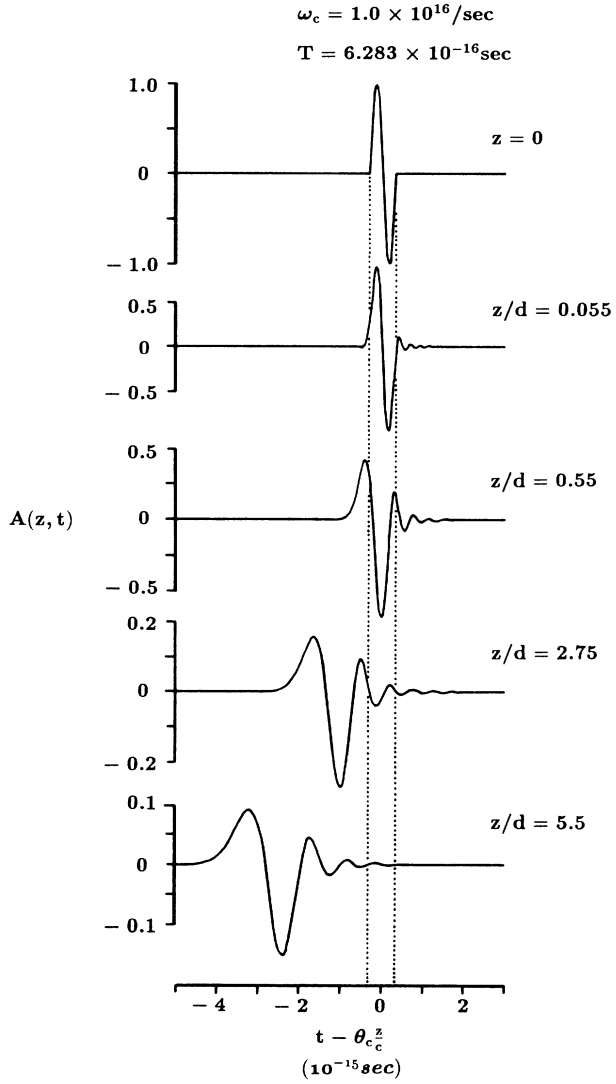

FIG. 17. Dynamical evolution of the propagated field due to an input rectangular modulated signal with below resonance carrier frequency $\omega_c=1.0\times 10^{16}$/sec and initial pulse width $T=6.283\times 10^{-10}$ sec in a strongly dispersive and absorptive medium. The e^{-1} penetration depth at this signal frequency is $d=1.82\times 10^{-4}$ cm.

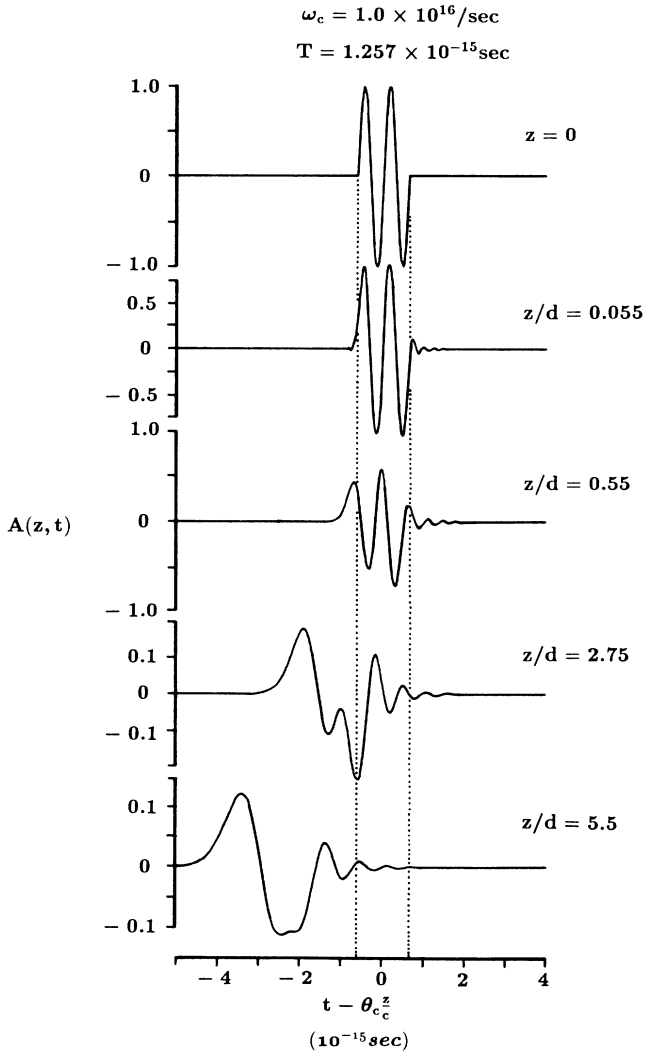

FIG. 18. Dynamical evolution of the propagated field due to an input rectangular modulated signal with below resonance carrier frequency $\omega_c=1.0\times 10^{16}$/sec and initial pulse width $T=1.257\times 10^{-15}$ sec in a strongly dispersive and absorptive medium.

time by the initial pulse width T. Since these two points in the field evolution experience no exponential decay[4-6] but rather decrease with the propagation distance only as $z^{-1/2}$, they will remain the prominent feature in the propagated field structure long after the signal contribution has attenuated away. This behavior applies throughout the below resonance frequency domain $\omega_c \in [0,\omega_0)$ and remains applicable up through most of the absorption band $\omega_c \in [\omega_0,\omega_1]$. In the upper region of the absorption band and for signal frequencies $\omega_c > \omega_1$ the Sommerfeld precursor becomes a dominant feature in the propagated waveform and must be included in any description of its overall temporal width.

The dynamical evolution of the propagated field at several increasing values of the propagation distance z is illustrated in Fig. 21 for the above resonance signal frequency $\omega_c = 1.0\times10^{17}$/sec, where $\omega_c > \omega_{SB}$. The e^{-1} penetration depth at this signal frequency is $d = 2.68\times10^{-5}$ cm. The initial pulse width here is $T = 6.283\times10^{-16}$ sec, which corresponds to ten oscillation periods of the signal. At the smallest propagation distance illustrated in the figure, $z/d = 0.037$ while at the intermediate propagation distance illustrated $z/d = 0.37$, so that these two propagated waveforms are in the immature dispersion regime. In both cases $cT/z > \theta_c - 1$ so that the pulse distortion is minimal. At the largest propagation distance illustrated in the figure $z/d = 3.73$, so that the propagated waveform is in the mature dispersion regime. In this last case $cT/z \approx \theta_{c1} - 1$, so that the prepulse is almost fully distorted (due to interference with the trailing edge Sommerfeld precursor) and the main pulse has disappeared, being replaced by the interfering

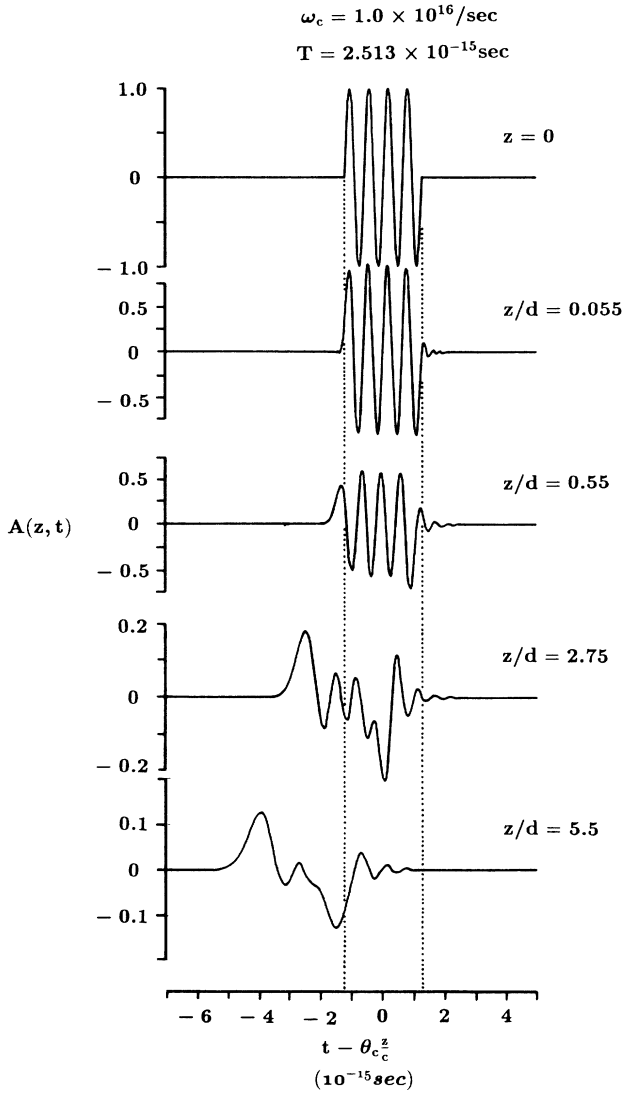

FIG. 19. Dynamical evolution of the propagated field due to an input rectangular modulated signal with below resonance carrier frequency $\omega_c = 1.0\times10^{16}$/sec and initial pulse width $T = 2.513\times10^{-15}$ sec in a strongly dispersive and absorptive medium.

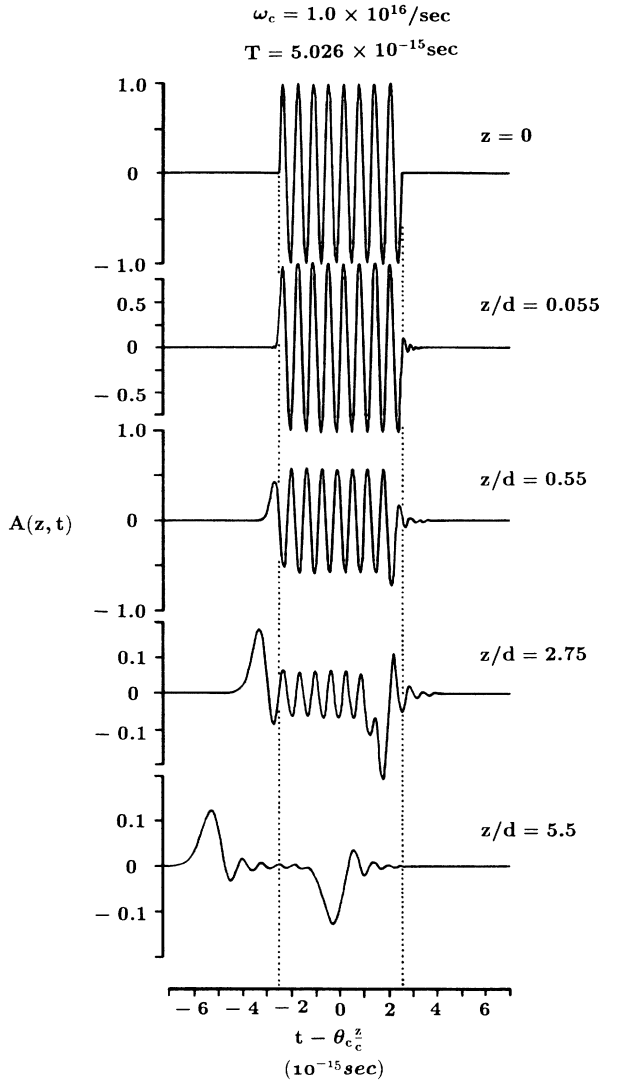

FIG. 20. Dynamical evolution of the propagated field due to an input rectangular modulated signal with below resonance carrier frequency $\omega_c = 1.0\times10^{16}$/sec and initial pulse width $T = 5.026\times10^{-15}$ sec in a strongly dispersive and absorptive medium.

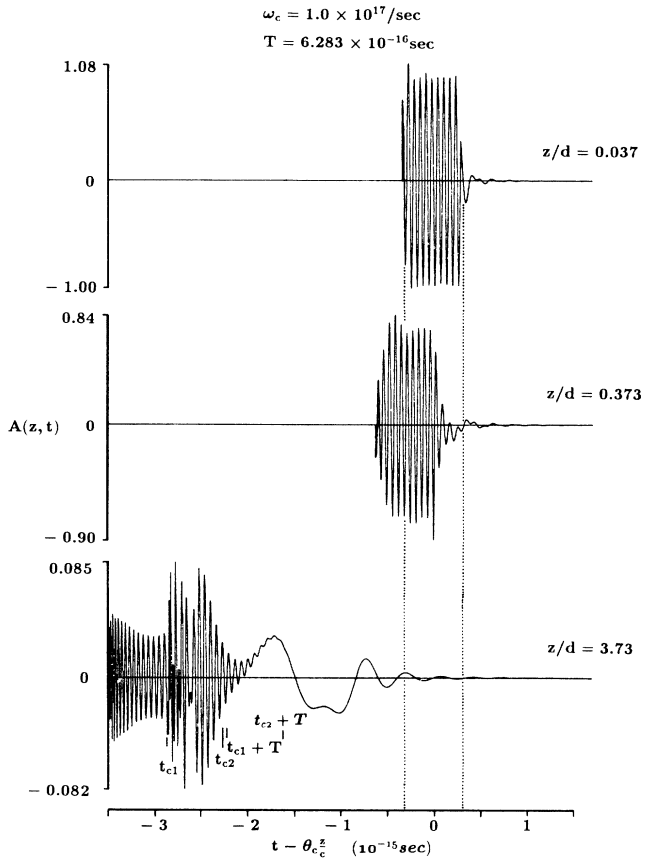

FIG. 21. Dynamical evolution of the propagated field due to an input rectangular modulated signal with above resonance carrier frequency $\omega_c = 1.0\times 10^{17}$/sec and initial pulse width $T = 6.283\times 10^{-16}$ sec in a strongly dispersive and absorptive medium.

Brillouin precursors. The time origin for each propagated waveform illustrated has been shifted by the amount $\theta_c z/c$, and the dotted lines in the figure depict the locations of the front and back of the initial, undistorted pulse which propagates at the main signal velocity $v_c = c/\theta_c$.

The temporal width Δt_s of the main pulse is then seen to decrease from T to zero as the propagation distance z increases from zero, as described by Eq. (6.5). In addition, the temporal width Δt_p of the prepulse is seen to first increase with increasing propagation distance z, as described by Eq. (6.4), and then decrease with increasing propagation distance z as the pulse distortion becomes severe, as described by Eq. (6.6). Nevertheless, the overall temporal width of the entire propagated waveform is seen to increase with the propagation distance z. If one includes just the high-frequency structure in the mature dispersion regime, which evolves over the θ domain from $\theta = 1$ to $\theta \approx \theta_0$, the overall temporal width is given by

$$\Delta t' \cong \frac{z}{c}(\theta_0 - 1), \quad \frac{c}{z}T < \theta_c - 1 , \tag{6.8}$$

while if one includes both the low- and high-frequency structure, which evolves over the θ domain from $\theta = 1$ to $\theta \simeq \theta_0 + (c/z)T$, the overall temporal width is found to be

$$\Delta t \cong T + \frac{z}{c}(\theta_0 - 1) , \tag{6.9}$$

which is valid for all $(c/z)T < \theta_c - 1$. Equation (6.8) is the appropriate measure of the overall propagated pulse width in the mature dispersion regime if one only detects the high-frequency content of the field, while Eq. (6.9) is the appropriate measure if one includes all significant frequency components.

VII. DISCUSSION

The uniform asymptotic description of dispersive pulse propagation presented here has, for the first time, provided a complete, accurate analytic description of rectangular pulse dispersion in a single-resonance Lorentz medium. This description is valid for arbitrary initial pulse widths T at any fixed input signal frequency $\omega_c \in [0, \infty)$ in the mature dispersion regime. The results clearly show that the resultant pulse distortion in a linear causally dispersive medium is primarily due to the precursor fields that are associated with the leading and trailing edges of the input pulse. Other approaches[15–19] to linear dispersive pulse propagation which rely upon the quasimonochromatic or some slowly varying envelope approximation neglect, by the very nature of their approach, these precursor fields and so cannot provide such an accurate description for either rapid rise-time pulses or ultrashort pulses. The central difficulty in these other approaches is that they expand the complex wave number $\tilde{k}(\omega)$ appearing in the integral representation of the propagated field in a Taylor series about the carrier frequency ω_c. For either rapid rise-time or ultrashort pulses the number of terms in this Taylor series expansion that is necessary to accurately describe the underlying dispersive pulse dynamics becomes prohibitively large from both a computational and physical point of view, while the first few lower-order terms completely misrepresent the physical processes involved. The asymptotic approach, on the other hand, expands the complex phase function $\phi(\omega,\theta)$ in a Taylor series about just those frequencies that provide the dominant contribution to the integral representation at each space-time point. This then results in an asymptotic series representation whose leading terms provide a completely accurate representation of the physical processes involved in dispersive pulse dynamics.

The analysis presented here is one important facet of a canonical theory of the dynamics of dispersive pulse propagation in causal media and systems. This analysis clearly rests upon the canonical problem of the unit-step-function-modulated signal whose complete solution has only recently been obtained for a single-resonance Lorentz medium[4–6] and finally extended to the more physically realistic case of a double resonance medium.[29] Taken together, these two asymptotic representations provide a valuable description of the dispersive pulse dynamics of both rapid rise-time signals and pulses of arbi-

trary initial time duration. In addition, they provide a correct, detailed description of the pulse velocity in the dispersive and absorptive medium that is not afforded by any other approach.

The next class of problems to be treated includes both finite rise-time signals and pulses of arbitrary time duration. Preliminary results for ultrashort Gaussian pulse propagation[30] once again prove the fundamental role that the precursor fields provide in the correct description of dispersive pulse dynamics.

ACKNOWLEDGMENTS

The research presented in this paper was, in part, supported by the United States Air Force Office of Scientific Research under Contract No. F49620-89-C-0057.

---

*Also with the Department of Mathematics and Statistics, University of Vermont.

[1]A. Sommerfeld, Ann. Phys. **44**, 177 (1914).

[2]L. Brillouin, Ann. Phys. **44**, 203 (1914).

[3]L. Brillouin, *Wave Propagation and Group Velocity* (Academic, New York, 1960).

[4]Kurt Edmund Oughstun, Ph.D. thesis, University of Rochester, 1978, available from University Microfilms International, Ann Arbor, MI.

[5]K. E. Oughstun and G. C. Sherman, J. Opt. Soc. Am. B **5**, 817 (1988).

[6]K. E. Oughstun and G. C. Sherman, J. Opt. Soc. Am. A **6**, 1394 (1989).

[7]G. C. Sherman and K. E. Oughstun, Phys. Rev. Lett. **47**, 1451 (1981).

[8]G. R. Baldock and T. Bridgeman, *Mathematical Theory of Wave Motion* (Halsted, New York, 1981), Chap. 5.

[9]L. A. Segel and G. H. Handelman, *Mathematics Applied to Continuum Mechanics* (Macmillan, New York, 1977), Chap. 9.

[10]I. Tolstoy, *Wave Propagation* (McGraw-Hill, New York, 1973), Chaps. 1–2.

[11]P. Wyns, D. P. Foty, and K. E. Oughstun, J. Opt. Soc. Am. A **6**, 1421 (1989).

[12]K. E. Oughstun, P. Wyns, and D. P. Foty, J. Opt. Soc. Am. A **6**, 1430 (1989).

[13]R. Loudon, J. Phys. **3**, 233 (1970).

[14]K. E. Oughstun and S. Shen, J. Opt. Soc. Am. B **5**, 2395 (1988).

[15]C. G. B. Garrett and D. E. McCumber, Phys. Rev. A **1**, 305 (1970).

[16]J. Jones, Am. J. Phys. **42**, 43 (1974).

[17]D. G. Anderson and J. I. H. Askne, Proc. IEEE **62**, 1518 (1974).

[18]D. Anderson, J. Askne, and M. Lisak, Phys. Rev. A **12**, 1546 (1975).

[19]D. Anderson and M. Lisak, Phys. Rev. A **35**, 184 (1987).

[20]K. A. Connor and L. B. Felsen, Proc. IEEE **62**, 1586 (1974).

[21]D. Censor, J. Phys. A **10**, 1781 (1977).

[22]N. D. Hoc, I. M. Besieris and M. E. Sockell, IEEE Trans. Antennas Propag. **AP-33**, 1237 (1985).

[23]H. M. Nussenzveig, *Causality and Dispersion Relations* (Academic, New York, 1972), Chap. 1.

[24]J. A. Stratton, *Electromagnetic Theory* (McGraw-Hill, New York, 1941), Sec. 5.18.

[25]F. W. J. Olver, Stud. Appl. Math. Rev. **12**, 228 (1970).

[26]*Handbook of Mathematical Functions,* Natl. Bur. Stand. Appl. Math. Ser. No. 55, edited by M. Abramowitz and I. A. Stegun (U.S. GPO, Washington, D.C., 1964), p. 298.

[27]R. Barakat, J. Opt. Soc. Am. B **3**, 1602 (1986).

[28]R. Albanese, J. Penn, and R. Medina, J. Opt. Soc. Am. A **6**, 1441 (1989).

[29]S. Shen and K. E. Oughstun, J. Opt. Soc. Am. B **6**, 948 (1989).

[30]K. E. Oughstun, J. Laurens and P. Wyns, in *Asymptotic Description of Ultrashort Electromagnetic Pulse Propagation in a Linear Causally Dispersive Medium,* Proceedings of the 1989 International Union of Radio Science (URSI) International Symposium on Electromagnetic Theory, Stockholm, 1989 (The Royal Institute of Technology, Stockholm, 1989), pp. 497–499.